Article

SOURCE DATA | TRANSPARENT PROCESS | OPEN ACCESS

THE EMBO JOURNAL

The UBA domain of conjugating enzyme Ubc1/Ube2K facilitates assembly of K48/K63-branched ubiquitin chains

Lukas Pluska[1], Ernst Jarosch[1], Henrik Zauber[1], Andreas Kniss[2], Anita Waltho[1], Katrin Bagola[1], Maximilian von Delbrück[1], Frank Löhr[2], Brenda A Schulman[3], Matthias Selbach[1,4], Volker Dötsch[2] & Thomas Sommer[1,5,*]

Abstract

The assembly of a specific polymeric ubiquitin chain on a target protein is a key event in the regulation of numerous cellular processes. Yet, the mechanisms that govern the selective synthesis of particular polyubiquitin signals remain enigmatic. The homologous ubiquitin-conjugating (E2) enzymes Ubc1 (budding yeast) and Ube2K (mammals) exclusively generate polyubiquitin linked through lysine 48 (K48). Uniquely among E2 enzymes, Ubc1 and Ube2K harbor a ubiquitin-binding UBA domain with unknown function. We found that this UBA domain preferentially interacts with ubiquitin chains linked through lysine 63 (K63). Based on structural modeling, *in vitro* ubiquitination experiments, and NMR studies, we propose that the UBA domain aligns Ubc1 with K63-linked polyubiquitin and facilitates the selective assembly of K48/K63-branched ubiquitin conjugates. Genetic and proteomics experiments link the activity of the UBA domain, and hence the formation of this unusual ubiquitin chain topology, to the maintenance of cellular proteostasis.

Keywords cell stress; K48-linked; K63-linked; polyubiquitin; ubiquitin-conjugating enzymes

Subject Categories Post-translational Modifications & Proteolysis; Structural Biology

DOI 10.15252/embj.2020106094 | Received 29 June 2020 | Revised 22 December 2020 | Accepted 5 January 2021 | Published online 12 February 2021

The EMBO Journal (2021) 40: e106094

Introduction

Numerous processes in the eukaryotic cell rely on posttranslational modifications (PTMs) with the 76 amino acid protein ubiquitin (Ub). These PTMs regulate the half-life, cellular localization, binding of interaction partners, and/or activity of client proteins (Swatek & Komander, 2016). Due to the large number of enzymes involved and the multiple combinations through which they contribute to ubiquitin transfer, ubiquitination comprises a highly versatile and dynamic PTM system. In many cases, ubiquitin itself is ubiquitinated at any of its seven lysine residues or its N-terminus causing the formation of polymeric chains (Swatek & Komander, 2016). Depending on the linkage type, these ubiquitin chains have distinct properties and induce different biological outcomes. For example, polyubiquitin linked through lysine 48, which is the most abundant type in cells (Clague *et al*, 2015), typically targets client proteins to the 26S proteasome for degradation (Hershko & Ciechanover, 1998). In contrast, the second most frequent type under most conditions (Clague *et al*, 2015; Swatek & Komander, 2016)—K63-linked polyubiquitin—facilitates the assembly of protein complexes and therefore governs cellular processes such as DNA damage repair (Spence *et al*, 1995; Liu *et al*, 2018), transcriptional activation (Wang *et al*, 2001), innate immune responses (Gack *et al*, 2007), endocytosis (Gulia *et al*, 2017), or protein trafficking (Lauwers *et al*, 2009). The combination of different linkage types into mixed or branched polymers further expands the diversity of ubiquitin signals. The study of such heterogeneous chains is technically challenging, and reports on their biological significance and on the enzymatic machinery involved in their generation are scarce (Emmerich *et al*, 2013; Meyer & Rape, 2014; Wertz *et al*, 2015; Ohtake *et al*, 2016; Ohtake *et al*, 2018).

Modification of substrates with ubiquitin requires the coordinated and sequential activity of ubiquitin-activating enzymes (E1), ubiquitin-conjugating enzymes (E2), and ubiquitin ligases (E3). While E3 ligases typically confer substrate specificity, E2 ubiquitin-conjugating enzymes often determine the linkage type and spatial organization of the ubiquitin signal (Stewart *et al*, 2016). Recently, low-affinity interactions with the acceptor ubiquitin (Ub_A) mediated by ubiquitin-binding domains (UBDs) or other ubiquitin-binding

1 Max-Delbrück-Center for Molecular Medicine in the Helmholtz Association, Berlin-Buch, Germany
2 Institute of Biophysical Chemistry and Center for Biomolecular Magnetic Resonance, Goethe University, Frankfurt am Main, Germany
3 Department of Molecular Machines and Signaling, Max Planck Institute of Biochemistry, Martinsried, Germany
4 Charité – Universitätsmedizin Berlin, Berlin, Germany
5 Institute for Biology, Humboldt-Universität zu Berlin, Berlin, Germany
*Corresponding author. Tel: +49 30 9406 3753; E-mail: tsommer@mdc-berlin.de

interfaces outside the catalytically active UBC domain of E2 enzymes have emerged as key regulatory factors for the efficient assembly of ubiquitin chains (Wright *et al*, 2016; Watson *et al*, 2019). For example, the Cue1 protein recruits the K48-specific E2 enzyme Ubc7 to the tip of a ubiquitin chain through association with the penultimate ubiquitin moiety and therefore facilitates the elongation of K48-linked polyubiquitin (von Delbrück *et al*, 2016; Kniss *et al*, 2018). Similarly, the formation of K63-linked chains by Ubc13 relies on its cofactor Uev1a, which aligns the immediate Ub_A molecule with the active site of Ubc13 (Pastushok *et al*, 2005; Branigan *et al*, 2015).

Unlike other E2 enzymes, human Ube2K (E2-25K, HIP2) and its yeast homologue Ubc1 harbor a ubiquitin-associated domain (UBA domain), whose function has remained unclear. Ube2K has been linked to Huntington's disease (Kalchman *et al*, 1996; Pril *et al*, 2007), amyloid-β neurotoxicity (Song *et al*, 2003), and overcoming radiation-induced cell cycle arrest (Hong *et al*, 2019). Ubc1, in turn, is involved in protein turnover and essential for survival of yeast cells deleted for *UBC4* (Seufert *et al*, 1990). It was associated with vesicle biogenesis (Shieh *et al*, 2001), resistance to proteotoxic stress (Meena *et al*, 2011), transcription factor shuttling (Jiao *et al*, 2016), and protein quality control in the endoplasmic reticulum (Friedlander, *et al*, 2000) and in the nucleus (Ibarra *et al*, 2016). Furthermore, Ubc1 and Ubc4 were shown to act cooperatively in the degradation of substrates of the anaphase-promoting complex (APC/C; Rodrigo-Brenni & Morgan, 2007). Like other E2 enzymes, Ubc1 and Ube2K contain a catalytic core domain (UBC domain) of about 150 amino acids, which folds into a β-sheet of four antiparallel β-strands flanked by four α-helices (Stewart *et al*, 2016). While some E2 enzymes promiscuously conjugate ubiquitin to a wide range of polypeptides (e.g., Ubc4, Ubc6; Stoll *et al*, 2011; Weber *et al*, 2016), other E2 enzymes selectively target specific lysine residues within ubiquitin (e.g., Ubc7, Ubc13; Pastushok *et al*, 2005; von Delbrück *et al*, 2016). Ubc1 and Ube2K exclusively target K48 in ubiquitin for discharge, which has been attributed to the interaction of polar residues located around the active site in the UBC domain with polar residues within the acceptor ubiquitin molecule (Ub_A; Rodrigo-Brenni *et al*, 2010; Middleton & Day, 2015). Accordingly, the UBA domain is dispensable for the selective synthesis of K48-linked polyubiquitin (Rodrigo-Brenni & Morgan, 2007). The UBA domain also does not associate with the donor ubiquitin molecule (Merkley *et al*, 2005). Furthermore, conflicting data have been reported about the contribution of the UBA domain to enzymatic reactivity and processivity (Rodrigo-Brenni *et al*, 2010; Lee *et al*, 2018; Cook *et al*, 2020).

Here, we show that the UBA domain facilitates the formation of K48/K63-branched ubiquitin chains by Ubc1 and Ube2K. We present a structural model for the complex architecture underlying the reaction and link this activity to the resistance to proteotoxic stress in living cells. Our study corroborates the pivotal role of low-affinity Ub_A binding sites for polyubiquitin chain formation and emphasizes the biological importance of branched ubiquitin chains.

Results

An *in silico* model of Ubc1 and Ube2K in complex with ubiquitin molecules provides a rationale for the selective assembly of K48/K63-branched ubiquitin chains

Initially, we hypothesized that the UBA domain facilitates the elongation of K48-linked ubiquitin chains by Ubc1 in a similar manner to the E2 enzyme Ubc7 and its cofactor Cue1. Therefore, we expected that Ubc1 preferentially interacts with K48-linked polyubiquitin. However, GST epitope-tagged full-length Ubc1 or its UBA domain alone showed stronger binding to K63-linked ubiquitin chains than to K48-linked ubiquitin chains in a semi-quantitative binding experiment using fluorescently labeled ubiquitin (Fig 1A, Appendix Fig S1). Both chain types interacted efficiently with the UBA domain of Dsk2, which displays no preferences for the binding of different ubiquitin chains (Raasi *et al*, 2005). The UBC domain of Ubc1 alone (Ubc1-ΔUBA) or the ubiquitin-binding-deficient Ubc1-LRV variant (aa179-181 QGF to LRV; Wilson *et al*, 2009**)** only bound similar amounts of polyubiquitin as the GST protein, which was used as a negative control. These findings indicated that K63-linked polyubiquitin is the preferred substrate of Ubc1.

To understand how Ubc1 interacts with acceptor ubiquitin (Ub_A), we aggregated published structural data on the Ubc1 homologue Ube2K (Wilson *et al*, 2009; Ko *et al*, 2010; Middleton & Day, 2015; Lee *et al*, 2018) and combined them into an *in silico* model of the E2 enzyme in complex with two ubiquitin molecules (Fig 1B). Our structure prediction incorporates three previously reported

Figure 1. *In silico* model of Ubc1/Ube2K in complex with ubiquitin (Ub) provides a rationale for selective targeting of K63-linked ubiquitin chains resulting in the assembly of K48/K63-branched chains.

A Binding of ubiquitin chains to immobilized GST-fusion proteins. Indicated proteins were purified from *E. coli* and incubated with equal amounts of preformed fluorescently labeled ubiquitin chains, which were either K48- or K63-linked. The fraction of ubiquitin chains interacting with the bait protein was analyzed by SDS–PAGE and fluorescence scan. Total fluorescence was quantified per lane and normalized to the first lane (rel. fluo.). Asterisk (*) indicates lane from the same gel that was cropped and moved.

B A structural model of Ube2K in complex with two ubiquitin molecules was created based on previously published data (Ko *et al*, 2010; Middleton & Day, 2015). The UBC domain associates via its active site cysteine with the side chain of K48 in the immediate acceptor ubiquitin molecule (Ub_A-prox). A second ubiquitin molecule (Ub_A-dist) binds the UBA domain through the conserved hydrophobic patch. Selected atoms were highlighted as spheres: C-atom in the carboxy group (C_C) of Ub_A-prox-G76, S-atom in E2 active site Cys, C_C in Ub_A-dist-L71, N-atoms (blue) in Ub_A-prox of ε-amino groups of lysine residues (N_ε) and in the backbone of M1 (N_α).

C–E A structure of Ubc1 was superimposed onto the model from (B). Key residues were highlighted as sticks for the binding interfaces (C) between the UBC domain and Ub_A-prox, (D) between the UBA domain and Ub_A-dist, and (E) between the UBC domain and UBA domain. Additionally, amino acids whose side chains contribute to the UBC/UBA binding interface were determined and classified into "hot spot" or "contributing" residues using the algorithm SpotOn (Melo *et al*, 2016; Moreira *et al*, 2017).

F Interatomic distances from L71-C_C in Ub_A-dist to G76-C_C in Ub_A-dist or to putative attachment sites in Ub_A-prox were measured for various known ubiquitin conformations. The six closest attachment sites are listed in ascending order.

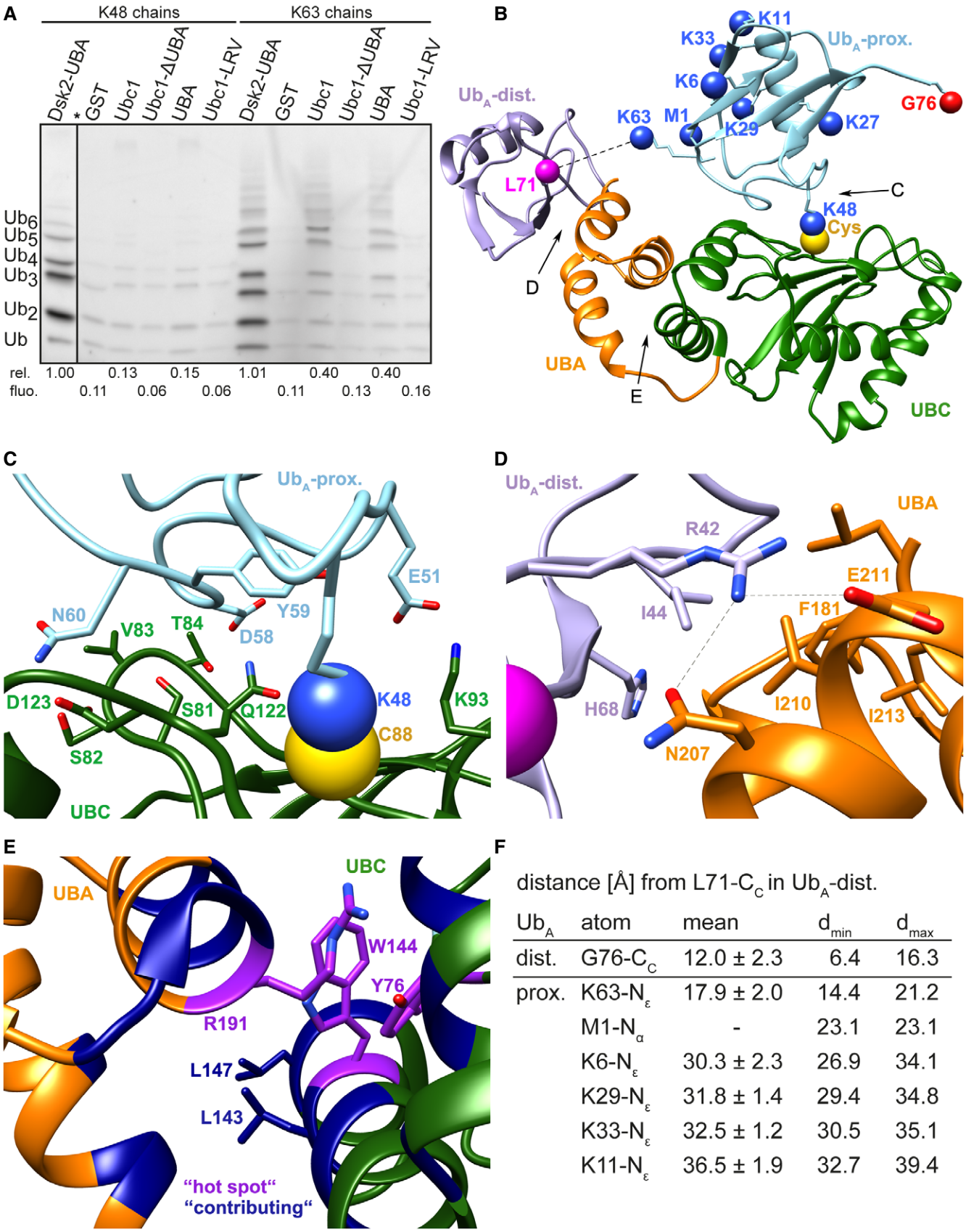

Ub$_A$	atom	mean	d$_{min}$	d$_{max}$
dist.	G76-C$_C$	12.0 ± 2.3	6.4	16.3
prox.	K63-N$_\varepsilon$	17.9 ± 2.0	14.4	21.2
	M1-N$_\alpha$	-	23.1	23.1
	K6-N$_\varepsilon$	30.3 ± 2.3	26.9	34.1
	K29-N$_\varepsilon$	31.8 ± 1.4	29.4	34.8
	K33-N$_\varepsilon$	32.5 ± 1.2	30.5	35.1
	K11-N$_\varepsilon$	36.5 ± 1.9	32.7	39.4

Figure 1.

binding interfaces: Ub/UBC domain (Fig 1C), Ub/UBA domain (Fig 1D), and UBA domain/UBC domain (Fig 1E). While the model was derived from X-ray crystallographic data of Ube2K, we superimposed a structure of Ubc1 (PDB: 1TTE) onto the final assembly (Fig 1C–E). The interaction of the UBC domain with the immediate acceptor ubiquitin (Fig 1C) was previously shown by HADDOCK modeling (Middleton & Day, 2015). Extensive mutagenesis studies in combination with activity assays validated the importance of the reported side chain interactions for the transfer of ubiquitin (Middleton & Day, 2015). In crystal structures of Ube2K in complex with ubiquitin (PDB: 6IF1, 3K9P), the binding of ubiquitin by the UBA domain involves the hydrophobic patch in ubiquitin and the helices α1 and α3 in the UBA domain (Fig 1D). The UBA domains of other proteins comprise equivalent binding interfaces with ubiquitin (Kozlov *et al*, 2007; Michielssens *et al*, 2014). Crystal structures of Ube2K (PDB: 5DFL, 6IF1, 3E46, 3F92, 3K9P) consistently show an interaction between the UBA domain and the UBC domain. We used the Phyre2 software (Kelley *et al*, 2015) to align the UBA and UBC domains of Ubc1 with this interface and the program SpotOn (Melo *et al*, 2016; Moreira *et al*, 2017) to assess the contribution of individual amino acid residues (Fig 1E).

In our analysis of the structural model, we observed that the C-terminus of ubiquitin bound to the UBA domain (Ub_A-dist) projected toward the ubiquitin molecule interacting with the UBC domain (Ub_A-prox), while the C-terminus of Ub_A-prox pointed away from Ub_A-dist (Fig 1B). The relative orientation of the two ubiquitin monomers implied that Ube2K could engage a diubiquitin molecule through simultaneous association of the UBC and UBA domains with the proximal and distal ubiquitin moieties, respectively. We hypothesized that such an architecture would facilitate the nucleophilic attack of the Ub_A-prox K48 side chain on the UBC~Ub thioester resulting in the formation of a branched ubiquitin polymer.

To assess which types of ubiquitin chains could be accommodated as the acceptor, we analyzed selected interatomic distances within the model (Fig 1F). The covalent bond that connects the two ubiquitin moieties of a diubiquitin molecule positions the carboxy C-atom (C_C) of Ub_A-dist G76 within 1.3 Å of the target N-atom in Ub_A-prox. Importantly, ubiquitin contains a highly flexible C-terminal region from L71 to G76 (Lange *et al*, 2008) and the dynamic rotameric states of the attachment sites need to be considered, too. To account for this, we first determined the distance between L71-C_C and G76-C_C to be within 6.4 - 16.3 Å in an NMR ensemble of 116 ubiquitin structures (PDB: 2K39). Next, we measured within our model the distance from L71-C_C of Ub_A-dist to various N-atoms of lysine ε-amino groups (N_ε) in Ub_A-prox for the 25 most frequent Lys rotamers (Shapovalov & Dunbrack, 2011), as well as to the amino-terminal N-atom located in M1. Only K63-N_ε in Ub_A-prox was sufficiently close (14.4 Å) to allow a covalent link between Ub_A-prox and Ub_A-dist. This finding further implicates K63-linked chains as a preferred substrate for Ubc1. M1-N_α—the next closest attachment site—was located at a distance of 23.1 Å.

The UBA domain facilitates the turnover of K63-linked ubiquitin and promotes the assembly of K48/K63-branched chains

To verify our structural model, we compared the enzymatic activity of Ubc1 toward various acceptor ubiquitin molecules. To this end, we monitored the transfer of fluorescently labeled monoubiquitin to excess amounts of C-terminally blocked acceptor ubiquitin (Fig 2A). Such single turnover ubiquitination experiments allowed us to follow the formation of a defined reaction product (Fig 2B). The relative fluorescence of this species was quantified and plotted over time to determine the reaction kinetics (Fig 2C). Using a linear fit, we obtained initial reaction rates for full-length Ubc1 or Ubc1-ΔUBA against a panel of acceptor ubiquitin molecules (Fig 2D, Appendix Fig S2). Ubc1 rapidly modified preformed K63-linked diubiquitin (K63-Ub_2), but not monoubiquitin or K48-Ub_2. The high initial reaction rate with K63-Ub_2 was dependent on the UBA domain and was not observed in samples containing Ubc1-ΔUBA (Fig 2D).

We then analyzed processing of K63-Ub_2 variants that had lysine 48 replaced by arginine (K48R) in either the distal, the proximal, or in both ubiquitin moieties. These substitutions remove the residue targeted for ubiquitination by Ubc1 in the corresponding ubiquitin molecule. Blocking this acceptor site in the proximal ubiquitin unit strongly impaired ubiquitin attachment by Ubc1, while the replacement of K48 in the distal moiety only had a minor impact (Fig 2D). This observation suggests that the UBA domain aligns Ubc1 with K63-Ub_2 in a directional manner. Next, we employed K63-Ub_2 with arginine 42 replaced by alanine (R42A) in either one or both ubiquitin molecules, which disrupts the binding to the UBA domain. While the introduction of R42A into the proximal ubiquitin had no effect on ubiquitination by Ubc1, the R42A exchange in the distal moiety strongly disrupted enzymatic turnover (Fig 2D). These data imply that the UBA domain binds the distal moiety in K63-Ub_2 to align the UBC domain with the proximal ubiquitin and therefore promotes the formation of K48/K63-branched ubiquitin molecules (Fig 2E).

The association of the UBC and the UBA domain facilitates formation of K48/K63-branched Ub chains

Our model predicts that the orientation of the UBA domain toward the UBC domain is a crucial determinant for the overall architecture of the Ubc1/Ub_A complex. However, the 17 amino acid stretch that connects these regions is a highly dynamic structure (Merkley & Shaw, 2004; Cook *et al*, 2015). Thus, we set out to identify defining features of the putative UBC/UBA binding interface and analyze their contribution to the activity of the enzyme. Sequence alignment with other E2 enzymes (Fig 3A) revealed that the residues W144 and Y76 in the UBC domain, which are predicted to be central constituents of the interaction interface (Fig 1E), are highly conserved. Therefore, these amino acids most likely contribute to the general E2 enzyme fold. However, at the positions corresponding to L143 and L147 in Ubc1, which according to our model also contribute to the hydrophobic UBC/UBA interface (Fig 1E), other E2 enzymes expose charged residues (Fig 3A). We therefore expressed and purified Ubc1 variants that contained glutamic acid at these sites and analyzed them with *in vitro* ubiquitination assays.

In agreement with our model, Ubc1(L143E) displayed reduced activity toward the K63-Ub_2 acceptor molecule (Fig 3B). In contrast, introduction of the L147E replacement did not diminish substrate processing. L147 is located at the fringe of the interface, and therefore, alterations of this site may cause only minor defects. The combination of the L143E and L147E substitutions had an additive effect on the activity of Ubc1 toward K63-Ub_2. Possibly, interactions between the side chains of the introduced glutamic acids resulted in

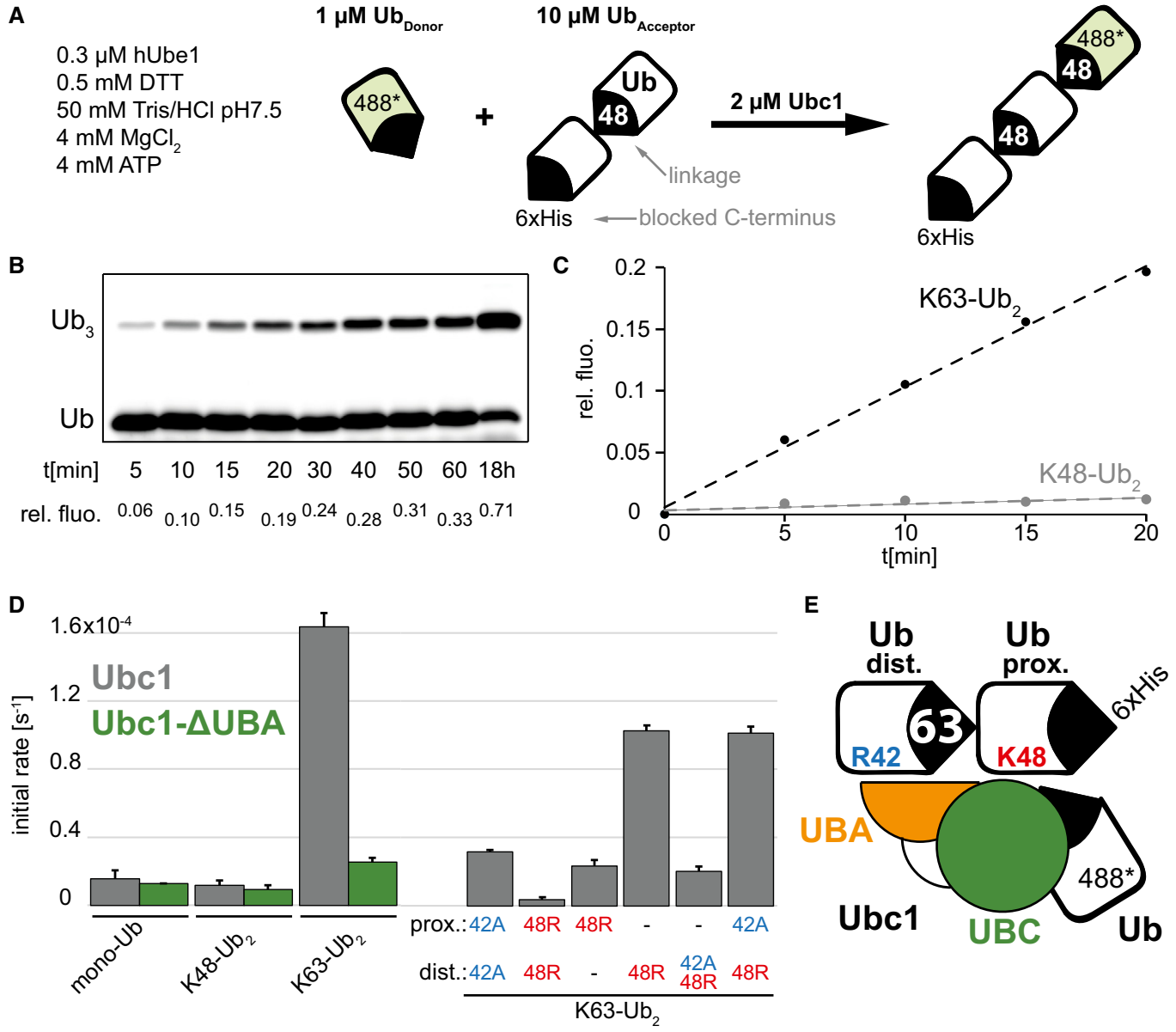

Figure 2. Enzymatic activity assays show the preferential targeting of K63-linked ubiquitin chains by Ubc1 resulting in the assembly of K48/K63-branched polyubiquitin.

A Reaction scheme for single turnover ubiquitination experiments with Ubc1 in the presence of fluorescently labeled monoubiquitin as donor and various C-terminally blocked acceptor ubiquitin molecules.

B At indicated time points, samples were taken from the reaction mix and analyzed by SDS–PAGE and fluorescence scan. Product fluorescence over total fluorescence per lane was quantified (rel. fluo.).

C The relative fluorescence was plotted over time for reactions with different ubiquitin acceptor molecules—for example in the presence of K63-linked diubiquitin ($K63\text{-}Ub_2$) or K48-linked diubiquitin. Initial reaction rates were determined as the slope of a linear fit of the fluorescence increase over 20 min.

D Initial reaction rates were determined for a panel of acceptor ubiquitin molecules in reactions with either full-length Ubc1 or Ubc1-ΔUBA (aa1-150). The binding of the UBA domain to individual ubiquitin molecules was disrupted by introducing an R42A amino acid exchange in ubiquitin, while acceptor sites were blocked by introducing the K48R substitution. Reactions were performed in triplicate. Bars show mean and SEM. For representative scans, see Appendix Fig S2.

E Schematic transition state for the reaction of Ubc1 with K63-linked diubiquitin. Binding of the distal moiety in $K63\text{-}Ub_2$ to the UBA domain involves R42 in ubiquitin and enhances targeting of K48 in the proximal moiety for discharge of donor ubiquitin by the UBC domain. This results in the assembly of a K48/K63-branched chain.

a more profound disruption of the hydrophobic interface. With monoubiquitin as the acceptor, we observed an equally low turnover for all tested Ubc1 variants (Fig 3B). This indicates that substitution of the leucine residues and the consequential changes in the relative positioning of the UBA and the UBC domains predominantly affect the K48/K63-branching activity of the enzyme.

The region, which connects the UBC and the UBA domain, is eleven amino acids (aa) longer in Ubc1 (aa151-167) than in Ube2K

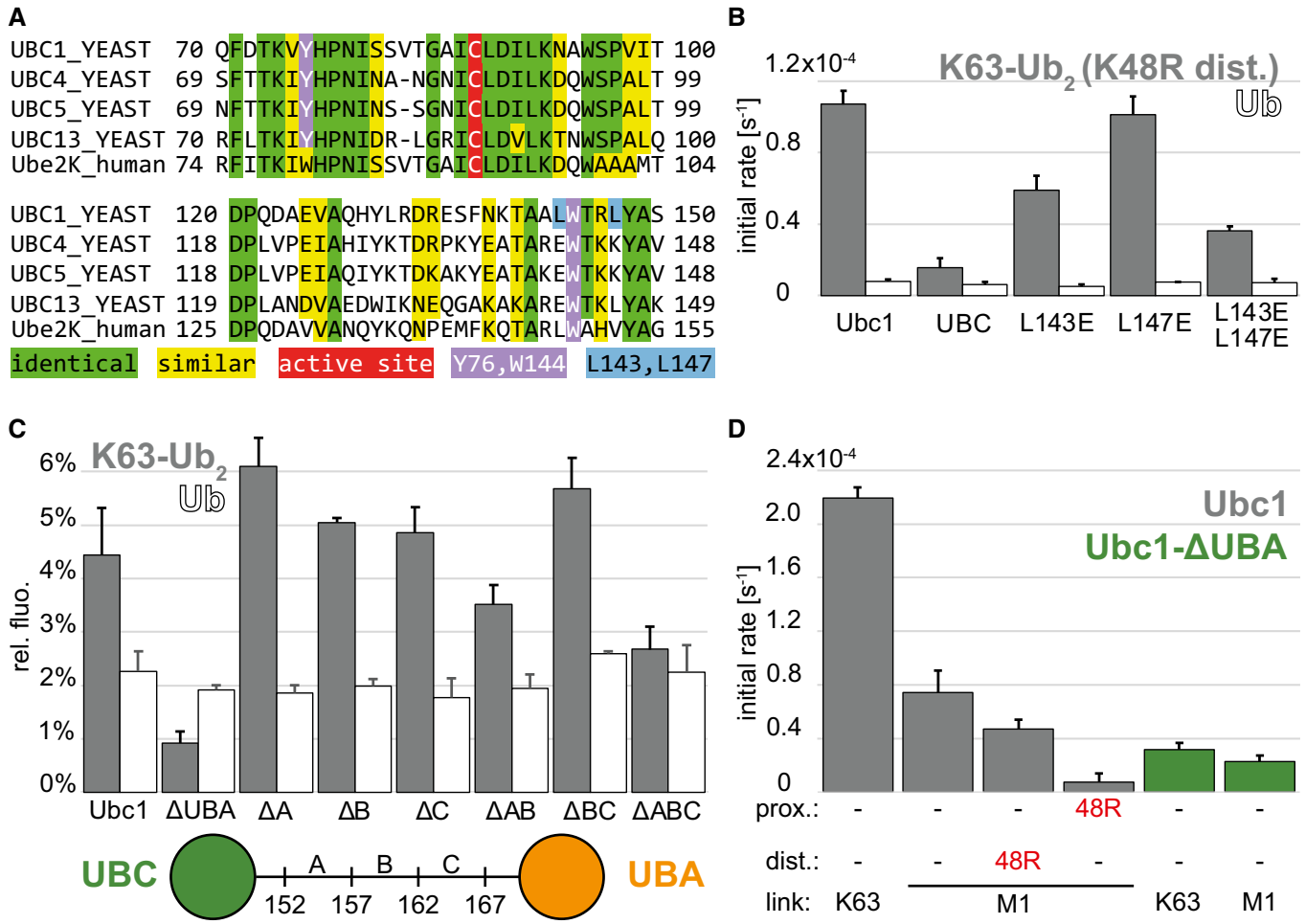

Figure 3. Branched chain formation by Ubc1 relies on the association of the UBA domain with the UBC domain and is selective for K63-linked chains.

A Residues associated with the binding of the UBA domain to the UBC domain were analyzed through sequence alignment of Ubc1 with other E2 enzymes from *S. cerevisiae*. Y76 and W144 in Ubc1 were predicted to be hot spot residues of the interface, while L143 and L147 were classified as contributing amino acids (Fig 1E).

B L143E and/or L147E amino acid substitutions were introduced into Ubc1 to disrupt the hydrophobic UBC/UBA domain interface. Single turnover ubiquitination experiments were performed with these Ubc1 variants in the presence of K63-Ub_2 with Ub(K48R) at the distal position or monoubiquitin as acceptor. Experiment and initial rate determination as described in Fig 2.

C Ubc1 variants were generated with deletions in the linker region (aa152-167), which connects the UBA domain and the UBC domain. Single turnover ubiquitination reaction mixes were incubated for 5 min with K63-Ub_2 or for 20 min with monoubiquitin as acceptor. Final product formation was analyzed by SDS–PAGE and fluorescence scan. Product fluorescence over total fluorescence (rel. fluo.) was quantified.

D C-terminally blocked M1-linked diubiquitin with or without a K48R amino acid substitution at the distal or proximal position was employed in single turnover experiments with full-length Ubc1 or Ubc1-ΔUBA. Reactions with acceptor K63-Ub_2 were carried out as controls. Initial rate determination as described in Fig 2.

Data information: All reactions were performed in triplicate. Bars show mean and SEM. For representative scans for the experiments shown in panels (B-D), see Appendix Fig S3A–C.

(aa154-159). Yet, the association of the UBC domain with the UBA domain places both ends of the linker in close proximity on the same side of the complex (Fig 1B). We therefore hypothesized that shortening of the linker should not affect the formation of the UBC/UBA interface and accordingly should also not interfere with the turnover of K63-Ub_2. Thus, we generated Ubc1 variants lacking stretches of five amino acids (aa152-156, aa157-161, aa162-166) or combinations thereof and analyzed their ability to ubiquitinate K63-Ub_2. Consistent with the model, removal of any five or the last ten amino acids (aa157-166) did not reduce product formation (Fig 3C). Deletion of the complete linker region or of the amino acids 152-161 impaired the reaction to some extent, but these Ubc1 variants were still significantly more active toward K63-Ub_2 than Ubc1-ΔUBA. Product formation with acceptor monoubiquitin was unchanged for the linker deletion variants implying that the overall catalytic activity of Ubc1 was not disturbed.

The association of the UBC and the UBA domain creates a binding interface, which restricts the possible conformations of a diubiquitin molecule that engages both domains at the same time. This limitation provides an attractive explanation for the selective targeting of K63-linked chains by Ubc1. To gain further insights into the substrate specificity of the enzyme, we investigated the turnover of

linear ubiquitin chains by Ubc1 with an *in vitro* ubiquitination assay (Fig 3D). In these molecules, the carboxy-terminal glycine (G76) of ubiquitin is attached to the amino-terminal methionine (M1) of the next ubiquitin moiety. Linear polyubiquitin adopts so-called open conformations that are highly similar to those of K63-linked chains (Wang *et al*, 2014). Moreover, after K63, M1 is the second closest attachment site to connect Ub_A-prox and Ub_A-dist in our model of a diubiquitin molecule bound to Ubc1 (Fig 1F). Compared with the processing of K63-Ub_2, we measured approximately three times lower initial reaction rates of Ubc1 in the presence of M1-Ub_2 as an acceptor (Fig 3D). Interestingly, a significantly higher initial reaction rate was observed for M1-Ub_2 containing Ub(K48R) at the distal rather than at the proximal position. This mirrors the preference of Ubc1 to discharge ubiquitin onto the proximal moiety of K63-Ub_2. In summary, M1-linked polyubiquitin can also serve as an acceptor for branched chain synthesis by Ubc1 *in vitro*, but it represents a poor substrate compared with K63-linked chains.

To further investigate the contribution of the UBA domain to the enzymatic properties of Ubc1, we created variants of this enzyme harboring different ubiquitin-binding domains. To this end, we replaced the UBA domain with either the CUE domain of Cue1, which specifically associates with K48-linked chains, or the Dsk2 UBA domain, which displays no preference but higher affinity for the binding of different polyubiquitin molecules (Fig EV1A). We tested these chimeric constructs in endpoint experiments employing different acceptor ubiquitin molecules (Fig EV1B). No substitution significantly increased total product formation. This supports the idea of an intricate role of the UBA domain in enzyme activation beyond merely increasing the local concentration of Ub_A at the UBC domain of Ubc1.

Characterization of UBA domain binding to differently linked polyubiquitin by NMR spectroscopy

The CUE domain of Cue1 preferentially associates with the proximal moieties in K48-linked chains, which facilitates chain elongation by Ubc7 (von Delbrück *et al*, 2016). Based on the results of the activity assays with Ubc1, we speculated that the UBA domain in Ubc1 also exhibits distinctive ubiquitin-binding properties. To investigate this in more detail, we synthesized K48-Ub_2 and K63-Ub_2 containing ^{15}N-labeled moieties at either the proximal or the distal position. Upon titration with unlabeled UBA domain, binding events at those positions were analyzed by NMR spectroscopy (Fig 4A–D). The strongest chemical shift perturbations (CSPs) were recorded for amino acids within the hydrophobic patch of ubiquitin (I44, L8, G47, V70, R42, H68). Interestingly, we also observed a pronounced CSP of K48 in ubiquitin indicating that this residue contributes to binding of the UBA domain. As shown for other systems, such an interaction can compete with the enzymatic activity of UBC domains (Kniss *et al*, 2018). By employing a model based on two different binding sites in diubiquitin (Raasi *et al*, 2005), we quantitatively analyzed the NMR titration experiments and calculated K_D values (Fig 4E and F). For the binding of the UBA domain to monoubiquitin, a previous study reported a K_D value of (228 ± 68 μM; Merkley & Shaw, 2004). We determined comparable K_D values of (188 ± 20 μM) and (192 ± 13 μM) for the proximal and distal moiety in K63-Ub_2, respectively. Compared with K63-Ub_2, the binding affinity for the distal moiety in K48-Ub_2 was equal within error (259 ± 58 μM) but lower for the proximal moiety (382 ± 98 μM). This may be explained by the involvement of the Ub K48 side chain in establishing the Ub/UBA interaction, which is blocked in all but the most distal moiety of a K48-linked chain. The reduced affinity toward K48-linked polyubiquitin and the role of Ub K48 in the binding interface challenge a selective function of Ubc1 in the formation of homotypic K48-linked ubiquitin chains.

The distinct ubiquitin-binding properties of the Cue1 CUE domain and the Ubc1 UBA domain may also be explained by the different requirements for ubiquitin chain elongation and branched chain formation, respectively. Chain elongation involves the iterative interaction of the E2 enzyme with the most distal ubiquitin moiety. However, the relative abundance of this ubiquitin molecule decreases proportionally with the length of the ubiquitin chain, and in consequence, productive binding events become increasingly unlikely. Selective binding to a particular ubiquitin moiety as described for the CUE domain in Cue1 and the subsequent recruitment of the cognate E2 enzyme Ubc7 to the tip of a ubiquitin chain can compensate this effect (von Delbrück *et al*, 2016). In contrast, the introduction of a branching point can occur at any proximal ubiquitin molecule in the chain. Therefore, the number of possible attachment sites and thus the chance for productive binding events increase with the length of the polymer. This renders the binding to a specific position less important for branching.

Branched chain assembly by Ubc1 is conserved among species and outperforms *de novo* chain synthesis

To further explore the enzymatic properties of Ubc1 and its homologues Ube2K (human) and ubc-20 (*C. elegans*), we performed single turnover ubiquitination experiments and directly compared the activity of these enzymes with the *bona fide* chain building E2 enzymes Ubc7 and Ubc13 (Fig 5A–C). Ubc7/Cue1 displayed overall higher activity than Ubc1 in these assays. For example, the elongation of K48-Ub_2 by Ubc7/Cue1 was approximately 50 times faster than by equimolar amounts of Ubc1. However, the modification of K63-Ub_2 occurred only with two times higher rates. Moreover, Ubc1 showed eleven times higher initial reaction rates for its preferred substrate (K63-Ub_2) over the best off-target molecule (monoubiquitin), while Ubc7 only showed a twofold higher rate (K48-Ub_2 versus K63-Ub_2). These observations emphasize the high selectivity of Ubc1 for the processing of K63-Ub_2. Similar to Ubc1, Ube2K and ubc-20 displayed significantly higher initial reaction rates for K63-Ub_2 with Ub(K48R) at the distal rather than at the proximal position. In contrast, Ubc13/Uev1a modified both acceptor molecules equally fast. This indicates that the presented mechanism for K48/K63-branched chain formation is conserved among species.

Ultimately, we aimed to assess the ability of Ubc1 to form ubiquitin chains *de novo* and to compare it with its propensity to generate branched polyubiquitin (Fig 6A). In an *in vitro* ubiquitination assay with fluorescently labeled monoubiquitin as the only ubiquitin entity, Ubc1 mainly synthesized diubiquitin and to a lesser extent higher molecular weight products over time (Fig 6B). We did not observe a stepwise increase in the size of the products, and thus, we assume that at least some of the larger species arose from the *en bloc* transfer of smaller chains or represent ubiquitinated forms of the enzymes in the reaction. The overall fluorescence intensity of the products synthesized by Ubc1-ΔUBA was similar to that generated by full-

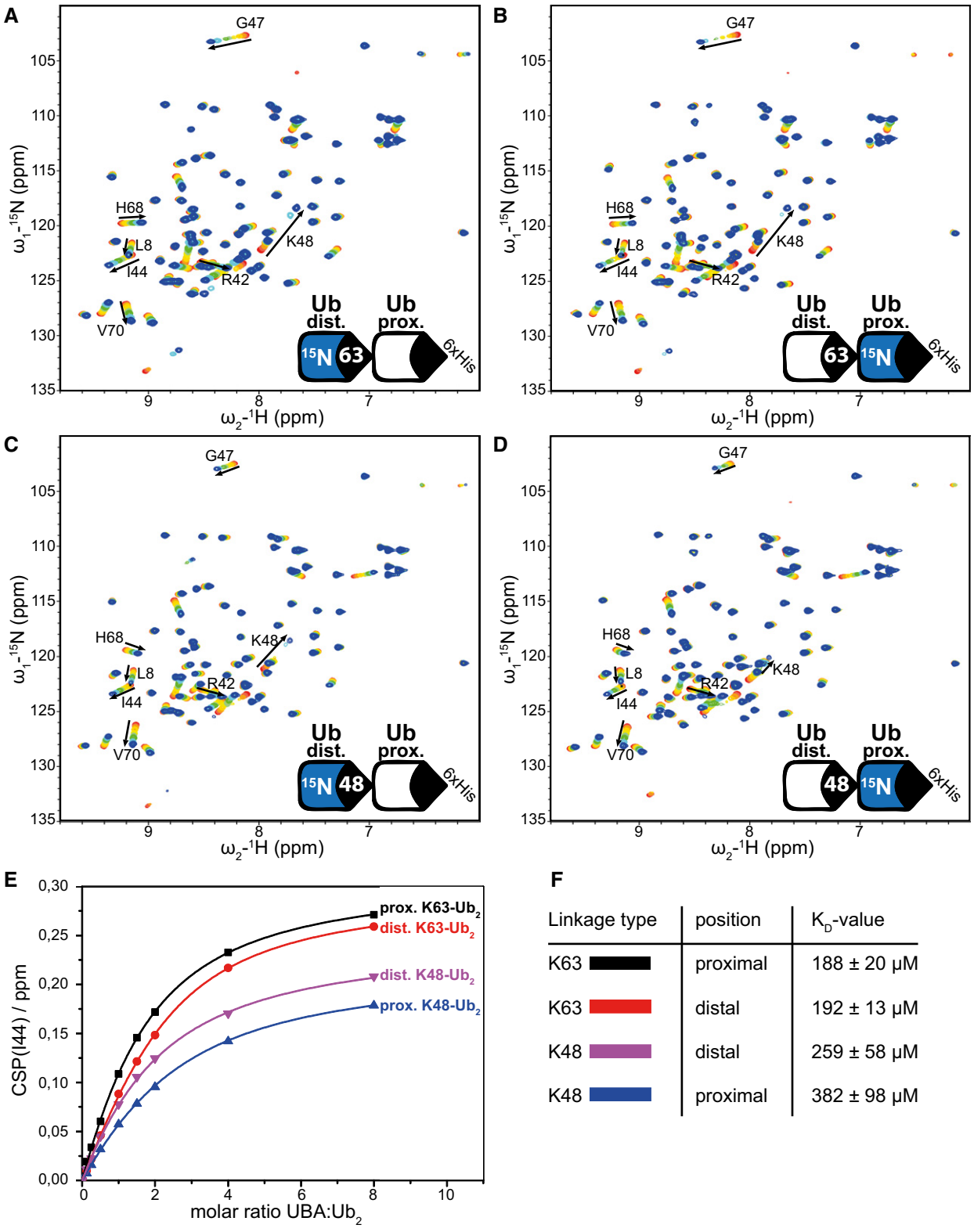

Figure 4. Interaction analysis of individual ubiquitin moieties in K48-Ub$_2$ or K63-Ub$_2$ with the UBA domain of Ubc1.

A–D ^{15}N-labeled diubiquitin probes were titrated with the UBA domain up to molar ratio of 8:1 (UBA : Ub$_2$). NMR spectra were recorded for (A) the distal moiety in K63-Ub$_2$, (B) the proximal moiety in K63-Ub$_2$, (C) the distal moiety in K48-Ub$_2$, or (D) the proximal moiety in K48-Ub$_2$.

E CSPs of I44 were plotted over UBA domain concentration.

F K$_D$ values for binding of the UBA domain were determined from results in (E) assuming two independent but different binding sites.

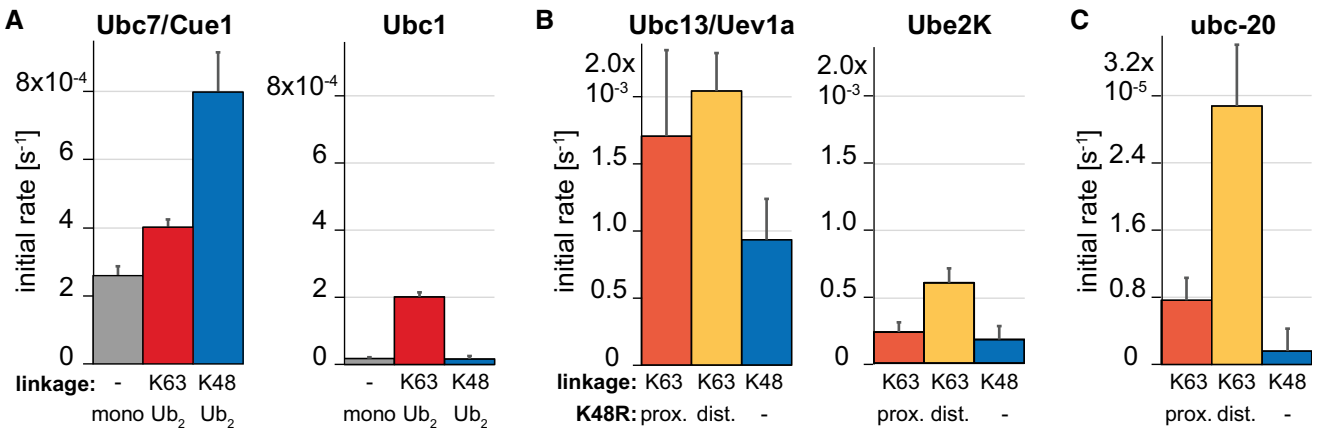

Figure 5. Branched chain formation by Ubc1 is conserved among species. Ubc1 is slower but more selective than bona fide chain building E2 enzymes.

A The activity of Ubc1 was compared with the K48-linked chain building enzyme Ubc7/Cue1 in single turnover ubiquitination experiments in the presence of either monoubiquitin, K48-Ub_2, or K63-Ub_2. Initial rates were determined as described in Fig 2.

B The K63-linked chain building enzyme Ubc13 with its cofactor Uev1a or the Ubc1 homologue Ube2K (*h. sapiens*) was employed in single turnover ubiquitination experiments in the presence of K63-Ub_2 with Ub(K48R) at the proximal or distal position or in the presence of K48-Ub_2. Initial rate determination as described in Fig 2.

C Experiment as in (B) but with the Ubc1 homologue ubc-20 (*C. elegans*).

Data information: All reactions were performed in triplicate. Bars show mean and SEM. For representative scans of gels from the experiments shown here, see Appendix Fig S3D and E.

length Ubc1. However, in reactions containing Ubc1-ΔUBA we detected larger amounts of high molecular weight ubiquitin conjugates (Fig EV2A). Full-length Ubc1 may be less capable to produce such species, because the discharge of preformed ubiquitin chains *en bloc* is less efficient due to their interaction with the UBA domain (Cook *et al*, 2020). Next, we set up reactions containing Alexa 488-labeled ubiquitin and a threefold lower concentration of Alexa 647-labeled K63-linked Ub_3 as an acceptor molecule (Fig 6C). In consequence, both molecules contributed to equimolar amounts of ubiquitin moieties in these assays. By overlaying scans of both fluorescence channels, we compared the capabilities of full-length Ubc1 and Ubc1-ΔUBA to modify K63-Ub_3 or to synthesize polyubiquitin *de novo*. While Ubc1-ΔUBA targeted both ubiquitin species with almost equal efficiency, the full-length enzyme formed significantly more product with the K63-Ub_3 acceptor. This indicates that the UBA domain increases the likelihood for productive binding of Ubc1 to the K63-Ub_3 acceptor, which is in line with our model for branched chain synthesis. We speculate that with sufficiently high substrate concentrations, branched chain formation should significantly outcompete *de novo* chain formation by Ubc1. However, such an experiment is not feasible due the relatively high K_m value of the enzyme (473 μM for Ube2K; Middleton & Day, 2015).

In an approximation, we performed endpoint analyses of reactions in the presence or absence of K63-linked Ub_4 as an acceptor at a 1:4 molar ratio to fluorescently labeled donor ubiquitin (Fig 6D). For *de novo* chain formation with only fluorescent monoubiquitin, we again observed more high molecular weight product formation by Ubc1-ΔUBA than by full-length Ubc1 (lane 1). These reaction products were resistant to treatment with the K63-specific deubiquitinating enzyme AMSH (lane 4). To determine the product pattern resulting from modification of K63-Ub_4, we employed methylated ubiquitin, which can serve only as donor in the reaction (lane 2). As expected, significantly more product was formed by full-length Ubc1 than by Ubc1-ΔUBA. Moreover, prominent signals for one to three times modified K63-Ub_4 could be observed, while the UBC domain alone mostly transferred one and to a lesser extent two moieties. Upon AMSH treatment, the reaction products were shortened to diubiquitin indicative of multiple monoubiquitination of the K63-linked chain (lane 5). Combining unmethylated donor ubiquitin and the K63-Ub_4 acceptor in a reaction with Ubc1-ΔUBA (lane 3) resulted in a product pattern closely resembling an overlay of the control reactions (lane 1 and 2). In contrast, the product pattern for full-length Ubc1 (lane 3) mostly resembled the modification of K63-Ub_4 and showed reduced formation of Ub_2 and of high molecular weight K48-linked chains. AMSH treatment yielded mostly diubiquitin showing that Ubc1 predominantly introduces multiple branching points into the K63-linked chain instead of extending K48-linked chains from the K63-linked chain as scaffold (lane 6). In summary, these results demonstrate a preference for branching over processive chain assembly by Ubc1.

Specific cellular functions of Ubc1 require the UBA domain

To evaluate the biological significance of our findings, we aimed to verify the formation of K48/K63-branched chains in *S. cerevisiae*. Mass spectrometric detection of such ubiquitin species is enabled by the substitution of R54 in ubiquitin with alanine (Ohtake *et al*, 2016), which removes a trypsin cleavage site (Fig EV3A). We prepared a reference peptide and a spectral library accordingly (Fig EV3B and C). Ultimately, we detected the distinct marker peptide in lysates of yeast cells expressing Ub(R54A) but not in a control strain expressing Ub(R54A,K63R; Fig EV3D).

We next replaced the endogenous *UBC1* gene in yeast with a version encoding Ubc1-EA, which instead of E211 and E212

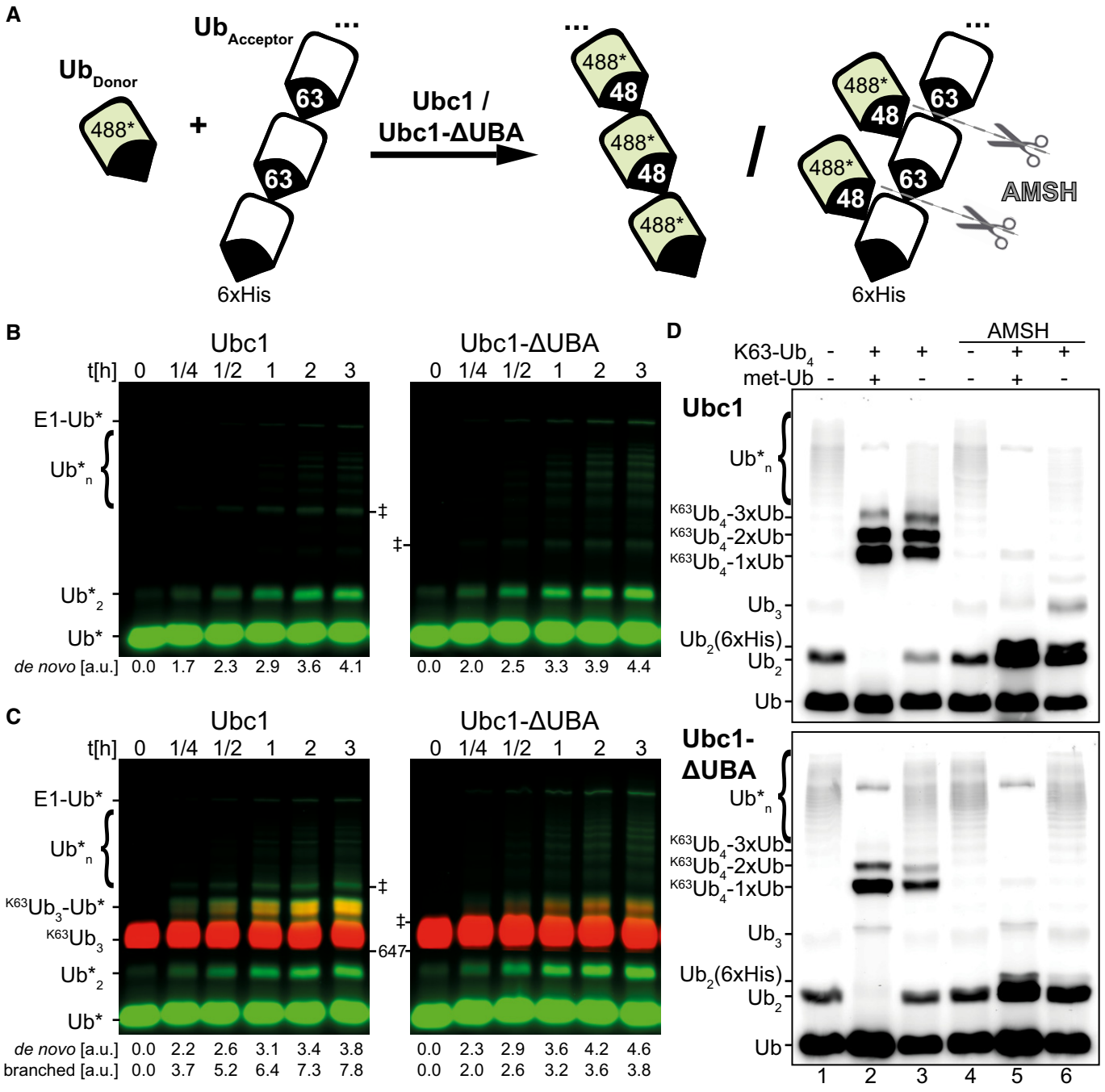

Figure 6. Branched chain formation by Ubc1 outperforms its capacity for *de novo* chain synthesis.

A Cartoon representation of reaction conditions used in (B–D), which simultaneously enable *de novo* chain assembly and the formation of K48/K63-branched chains.

B *In vitro* ubiquitination reactions with full-length Ubc1 or Ubc1-ΔUBA were performed. Samples were taken at indicated time points and analyzed by SDS–PAGE and fluorescence scan. Free chain synthesis from Alexa 488-labeled monoubiquitin was observed over time. Fluorescence of all reaction products was quantified and normalized to number of fluorophores per product ("*de novo*"). Double cross (‡) indicates ubiquitinated E2 enzyme.

C Reactions as in (B) were performed in the presence of C-terminally capped and Alexa 647-labeled K63-linked Ub_3. Monoubiquitin and K63-Ub_3 were used in a 3:1 molar ratio. Analysis as in (B). Modification of K63-Ub_3 was identified through correlation of fluorescence channels and their fluorescence quantified in the 488 channel ("branched"). The image from the 647 channel was cropped below the point indicated by "647" (see Fig EV2).

D Alexa 488-labeled monoubiquitin and C-terminally capped K63-Ub_4 were used in a 4:1 molar ratio for *in vitro* ubiquitination reactions with full-length Ubc1 or Ubc1-ΔUBA. Where indicated, Alexa 488-labeled monoubiquitin was methylated prior to the reaction (met-Ub) to block *de novo* chain assembly. Reactions were incubated overnight and quenched, and half the reaction mix from each condition was treated with the K63-specific deubiquitinating enzyme AMSH (lanes 4-6). Samples were analyzed by SDS–PAGE and fluorescence scan.

contains alanine resulting in an impaired binding of K63-linked ubiquitin chains (Fig EV4A and B). Accordingly, Ubc1-EA displays a threefold reduction in reaction rate in the presence of K63-Ub_2 in single turnover experiments (Fig EV4C). Ubc1-EA is a stable protein when expressed from the endogenous promoter (Fig EV4D) unlike other investigated binding-deficient variants (Fig EV4E) or truncated variants of Ubc1 (data not shown). We then determined the relative abundance of K48-/K63-branched ubiquitin chains in *wild-type* versus *Δubc1* or *UBC1-EA* yeast cells by overexpression of 10xHis-Ub(R54A) from a plasmid and enrichment of ubiquitinated material from cell lysates by metal affinity chromatography (Fig 7A). We performed proteomics experiments using SILAC technology in order to obtain precise relative peptide-level fold changes (Ong *et al*, 2002). Peptides that exclusively originate from the K48-/K63-branched ubiquitin species were substantially less abundant in samples obtained from *Δubc1* cells compared with those from the *wild-type* background (Figs 7B and EV4F). It must be noted that the amount of other ubiquitin-derived peptides was also reduced albeit to a lesser extent. The overall perturbation of the ubiquitome landscape might be caused by a disruption of the pleiotropic functions associated with Ubc1. We did not detect significant differences in the quantity of any ubiquitin marker peptide in the lysates of cells harboring *UBC1-EA* when compared to *wild type* (Figs 7C and EV4F). Expression of Ubc1-EA does not cause a shift in total cellular ubiquitin, possibly because branched chain assembly by Ubc1 is triggered in response to specific stimuli or only affects a small number of substrates. The reduced reaction rate of Ubc1-EA with K63-linked chains observed *in vitro* could be mitigated by other factors in living cells.

To assess global perturbations in the *UBC1-EA* yeast strain, we used another SILAC-based proteomics approach (Fig 7D). 4364 unique proteins were identified in this experiment, of which 15 were less abundant and 29 were enriched in *UBC1-EA* cells compared with *wild type* (Fig 7E, Table EV1). We also recorded the proteomes after growth at an elevated temperature (37°C) and in a *Δubc4* deletion background (Table EV2). In the *UBC1-EA* strain, significantly lower amounts of the NAD^+-dependent histone deacetylase Hst1 were detected, while various gene products for which Hst1 serves as a transcriptional repressor (Bedalov *et al*, 2003) including five Bna proteins, Sps19, and Tna1 were increased. This indicates a function of Ubc1-mediated branched ubiquitin chain formation in chromatin remodeling, which is supported by recent reports of an involvement of the human homologue Ube2K in this process (Fatima *et al*, 2020). We also found that 12 proteins with decreased abundance in the *UBC1-EA* strain are associated with cellular stress response pathways in the context of DNA replication (Tkach *et al*, 2012) and growth at elevated temperatures (Mühlhofer *et al*, 2019) (Fig 7D). Moreover, two key components of the heat shock response, Ssa4 (Mühlhofer *et al*, 2019) and Hsp12 (Welker *et al*, 2010), appeared to be adversely misregulated, when the *UBC1-EA* variant was combined with a deletion of the *UBC4* gene (Fig EV4G). Nevertheless, it remains unclear at this stage whether the observed change in abundance of these proteins in the *UBC1-EA* strain is caused by the disturbance of a particular cellular pathway or whether the pleiotropic functions of Ubc1 are disrupted in multiple processes.

To verify the results of the proteomic analysis, we assessed the growth of the *UBC1-EA* strain in the presence of the DNA damaging agent hydroxyurea (HU) and at an elevated temperature of 37°C (Fig 7F). Notably, the deletion of the *UBC1* gene was shown to cause a growth defect and to be synthetically lethal with a *UBC4* deletion (Seufert *et al*, 1990; Girard, *et al*, 2015). Moreover, expression of Ubc1-ΔUBA also does not yield viable cells in a *Δubc4* background (Girard *et al*, 2015). In this context, the UBA domain was suggested to mediate the recruitment of Ubc1 to the APC/C complex and to therefore fulfill essential functions during cell cycle progression. In contrast, the *UBC1-EA* strain showed normal growth and produced viable cells in combination with the deletion of the *UBC4* gene. However, growth of the *Δubc4/UBC1-EA* cells was strongly impaired in the presence of HU and at 37°C. Most likely, the deletion of *UBC4* aggravates physiological disruptions caused by *Ubc1-EA* due to their partially overlapping cellular functions (Seufert *et al*, 1990; Medintz *et al*, 1998; Hiraishi *et al*, 2006; Girard *et al*, 2015). Our data suggest that ubiquitin binding by the UBA domain and thus branched chain formation by Ubc1 are not essential for vegetative growth of yeast cells but play an important role in the maintenance of cellular proteostasis in response to acute stress.

Discussion

Non-covalent ubiquitin-binding interfaces, which coordinate the positioning of an acceptor ubiquitin (Ub_A) molecule, have emerged

Figure 7. Assembly of K48/K63-branched ubiquitin chains is conserved in *S. cerevisiae*. Yeast cells harboring ubiquitin-binding-deficient Ubc1 display specific proteomic alterations and are sensitized to stress conditions.

A A flowchart showing the sample preparation for the SILAC-based relative quantification of K48/K63-branched ubiquitin chains from yeast by mass spectrometry. 10xHis-Ub(R54A) was overexpressed in *wild-type* cells (*wt*) and either in cells deleted for *UBC1* (*Δubc1*) or cells expressing ubiquitin-binding-deficient Ubc1-EA. The R54A substitution in ubiquitin enables the production of a marker peptide for K48/K63-branched ubiquitin by trypsin digest, which can be detected by targeted proteomics (PRM).

B Log2-transformed fold changes of peptides between the *Δubc1* strain and *wild type* were determined. The forward and reverse SILAC experiments are shown on the x- or y-axis, respectively. The different ubiquitin marker peptides are indicated in the figure. For a list of fold changes, see Fig EV4F.

C Experiment as in (B) but for the *UBC1-EA* strain and *wild type*.

D A flowchart depicting the sample preparation for a SILAC-based proteomic shotgun experiment aimed to explore changes in protein abundance in Ubc1-EA-expressing yeast cells.

E Log2-transformed fold changes of proteins between the *UBC1-EA* strain and *wild type* were determined. The forward and reverse SILAC experiments are shown on the *x*- or *y*-axis, respectively. Genes, which were determined to be significantly different in their protein abundance, are marked in red and labeled. Asterisks (*) indicate genes, which are upregulated at a transcriptional and/or translational level upon heat stress (Mühlhofer *et al*, 2019). A double cross (‡) marks genes, for which the protein product changes in abundance and/or localization in response to DNA replication stress (Tkach *et al*, 2012).

F Ubc1-EA was genomically integrated into various yeast strains. Exponentially growing cells of the indicated genotype were spotted onto YPD plates in serial 10-fold dilutions. Where noted, cells were incubated at elevated temperature (37°C) or in the presence of hydroxyurea (HU) to induce DNA replication stress.

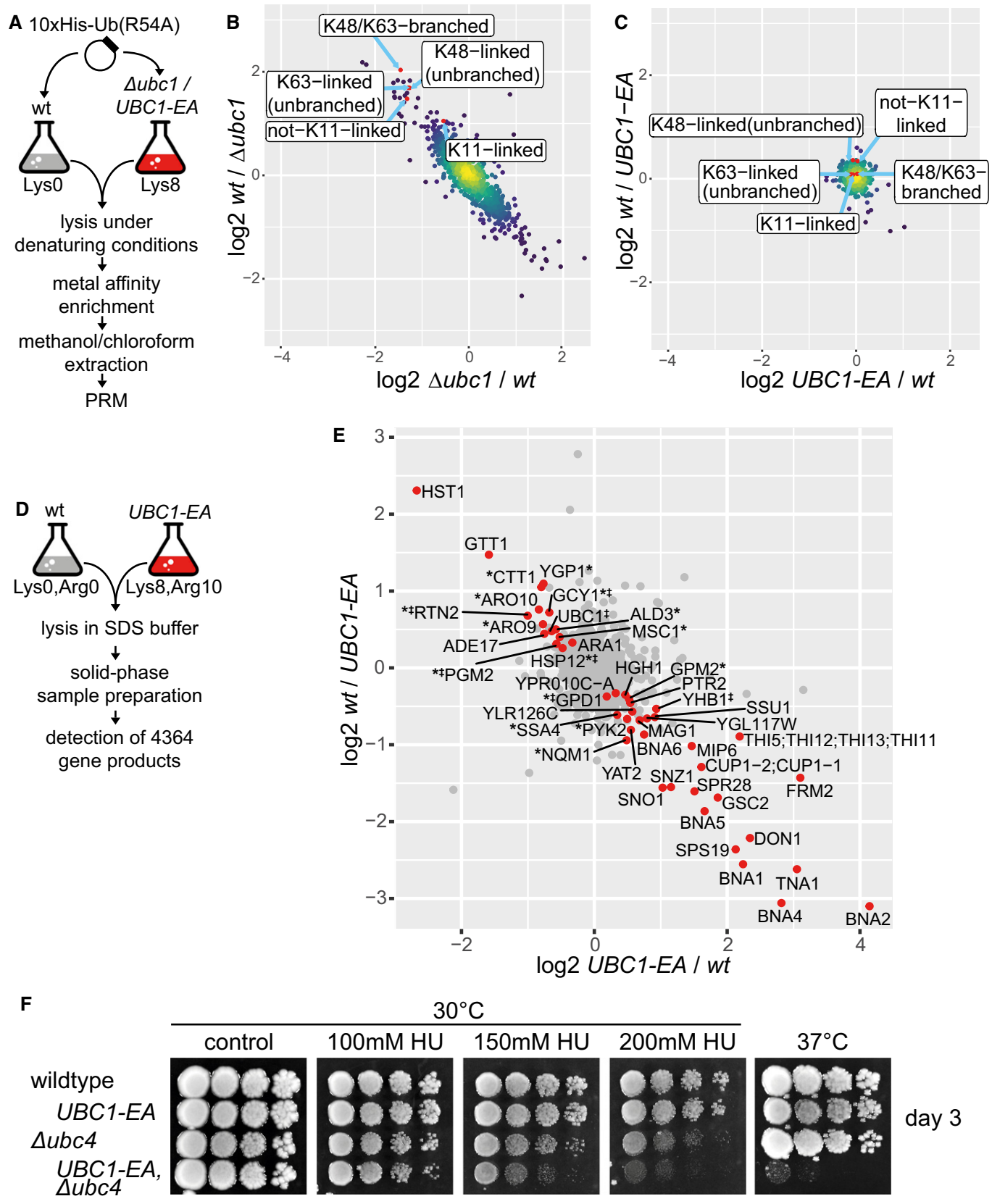

Figure 7.

as key regulatory factors of ubiquitin chain synthesis. In this study, we demonstrate through enzymatic activity assays that the ubiquitin-associated (UBA) domains of Ubc1 and Ube2K facilitate the rapid modification of K63-linked polyubiquitin to form K48/K63-branched chains—a thus far little-studied ubiquitin species. Based on previously reported data, we propose a structural model of Ubc1 and Ube2K during branched chain formation. Our model of the complex assembly also explains the selectivity toward K63-linked chains even over the structurally very similar M1-linked chains, which we observed for Ubc1. In detail, binding of the UBA domain to a distal ubiquitin moiety of a K63-linked chain facilitates the transfer of ubiquitin from the catalytic UBC domain to K48 of the adjacent proximal ubiquitin moiety. This requires coordination of the hydrophobic patch in the distal ubiquitin with the UBA domain via helix α1 and α3, association of UBC domain and UBA domain, and the alignment of the active site cysteine of the UBC domain with K48 in the proximal ubiquitin moiety. The latter interface is stabilized through interactions of polar side chains in Ub (D58-N60) and the UBC domain (S81/T84/D123 in Ubc1 and S85/T88/D127 in Ube2K; Rodrigo-Brenni *et al*, 2010; Middleton & Day, 2015).

Although the order of events during the formation of these interactions is unclear, we propose that an extension of the binding interface with Ub_A increases the dwell time of the enzyme at the substrate in an appropriate orientation and therefore enhances the likelihood for the transfer of the donor ubiquitin molecule. Alternatively, one could speculate that the backside binding of the UBA domain allosterically activates the UBC domain and that the two domains are drawn together through interaction with a K63-linked chain. Due to its low binding affinity, Ubc1, similar to the K48-linked chain elongating system Ubc7/Cue1, presumably associates with preexisting polyubiquitin conformations instead of inducing conformational remodeling (Kniss *et al*, 2018). The high K_D value of ~0.2 mM observed for the interaction of the UBA domain with Ub_A supports the idea that, in general, the dynamics of ubiquitin chain building systems rely on very transient binding events with Ub_A. Despite this low binding affinity, the UBA domains of Ubc1 and Ube2K appear to sufficiently stabilize the substrate interaction to counteract the inherently low reaction rates of Ubc1 and Ube2K, which we observed in comparison with other chain building E2 enzymes (Ubc7/Cue1 and Ubc13/Uev1a). Ubc1 and Ube2K may be less active yet more selective, because they contain glutamine as a so-called gateway residue close to the active site (Q122 and Q126, respectively). In contrast, other E2 enzymes typically harbor a leucine or alanine residue at this position (Valimberti *et al*, 2015; Rout *et al*, 2018). Glutamine as gateway residue has been proposed to form a critical interaction with Y59 in ubiquitin, which regulates the activity and selectivity of the ubiquitin transfer (Middleton & Day, 2015). In our experiments, we did not find evidence for a stimulating role of the UBA domain in *de novo* chain synthesis and in processive extension of homotypic K48-linked chains. The poor performance of Ubc1 in these functions supports the specificity for branched chain synthesis. Indeed, Ub K48 contributes to UBA domain binding, which may not only block the enzymatic acceptor site, but also interfere with the interaction of Ubc1 with proximal ubiquitin moieties in K48-linked chains. Consequently, this mode of binding should interfere with the recruitment and extension of K48-linked chains. We conclude that cellular pathways requiring the processive extension of K48-linked chains by Ubc1 or Ube2K should not involve the binding of the acceptor ubiquitin by the UBA domain.

Our work demonstrates that the formation of K48/K63-branched chains is conserved even in lower eukaryotes such as *S. cerevisiae*. At least one of only eleven E2 enzymes in this organism plays a designated role in their assembly. These observations underscore the biological significance of this little-studied protein modification for fundamental cell biological processes. In higher eukaryotes, K48/K63-branched chains appear to provide superior resistance against specific deubiquitinating enzymes compared with homotypic K63-linked chains in the context of NF-kB signaling (Ohtake *et al*, 2016). Moreover, K48/K63-branched chains have been associated with proteasomal degradation of substrates, which are initially decorated with K63-linked chains (Ohtake *et al*, 2018). Our genetic experiments in yeast link the UBA domain of Ubc1 and hence the generation of K48/K63-branched ubiquitin molecules to the maintenance of cellular proteostasis. Furthermore, our data indicate that Ubc4 should be involved in the formation of K63-linked chains as precursors for the branching activity of Ubc1. This could occur either directly through its ability to form short ubiquitin chains of various linkage types (Rodrigo-Brenni & Morgan, 2007) or through the interaction with a K63-specific E3 ligase (e.g., Rsp5; Stoll *et al*, 2011). Results of this study will pave the way for the identification of specific binders and substrates of K48/K63-branched ubiquitin, as well as for the exploration of conditions that induce their acute formation. Ultimately, such work will unravel the precise function of K48/K63-branched chain formation by Ubc1 and Ube2K in the living cell.

Materials and Methods

Model building and analysis

The structural model of Ube2K in complex with ubiquitin (Fig 1B) was created using UCSF chimera. A crystal structure of Ube2K, which contains UBC domain, UBA domain, and Ub_A-dist (PDB: 6IF1), served as initial framework. Other crystal structures of Ube2K (PDB: 5DFL, 3E46, 3F92, 3K9P) and crystal structures of different UBA domains in complex with ubiquitin (PDB: 2QHO, 4UN2) were superimposed onto 6IF1 to verify the validity of the interdomain interfaces. Ub_A-prox was added to the model according to a previously reported UBC domain/Ub_A-prox interface determined by HADDOCK modeling (Middleton & Day, 2015). Distances between key residues within the model were measured for various protein conformations using USCF chimera (Fig 1F). The UBC domain/UBA domain interface was modeled for Ubc1 with the Phyre2 web portal using the FASTA sequence of Ubc1 and a Ube2K crystal structure (PDB: 1YLA; Kelley *et al*, 2015). The UBC domain and UBA domain of a Ubc1 NMR structure (PDB: 1TTE) were individually superimposed onto the resulting complex (Fig 1C–E). The SpotOn web server (Melo *et al*, 2016; Moreira *et al*, 2017) was used to predict hot spot and contributing amino acid side chains of the UBC domain/UBA domain interface (Fig 1E). The amino acid sequence of Ubc1 was aligned with other E2 enzymes (Fig 3A) using Clustal Omega (Madeira *et al*, 2019).

Cloning and mutagenesis

Plasmids used in this study are listed in Table S1. A Ubc1 vector for recombinant expression in *E. coli* was generated by amplifying yeast genomic DNA and cloning into pGex6p1 via BamHI and SalI restriction sites. Point mutations were introduced into vectors using the QuikChange site-directed mutagenesis kit (Agilent Technologies) following the manufacturer's instructions. The identity of all plasmids was verified by sequencing.

Yeast strains

To establish the detection of K48/K63-branched chains, the yeast strain sub328 (genotype: *ubil-Δ1::TRP1 ubi2-Δ2::URA3 ubi3Δub-2 ubi4-Δ2::LEU2* +[pUB146] +[pUB100]), which harbors a single ubiquitin gene on plasmid pUB146, was modified (Spence *et al*, 1995). pUB146 was replaced with either pLP048 (expression of 10xHis-Ub-R54A) or pLP105 (expression of 10xHis-Ub-R54A,K63R) through negative selection on 5-Fluorouracil. All other yeast strains were haploid decedents of DF5 (genotype: *MATa/alpha trp1-1[am]/trp1-1 [am] his3-Δ200/his3-Δ200 ura3-52/ura3-52 lys2-801/lys2-801 leu2-3,-112/ leu2-3,-112*) that were generated following standard protocols (Longtine *et al*, 1998; Gueldener, 2002). Successful genetic modifications were validated by analytical PCRs and sequencing, as well as by SDS–PAGE and immunoblotting.

Recombinant protein purification

For heterologous protein expression, BL21 Rosetta cells were transformed with the desired expression plasmids (Table S1). Bacteria were grown at 37°C until OD600 of 1.0, cooled to 18°C, induced with 0.5 mM IPTG, and incubated overnight. Cells were pelleted, resuspended in lysis buffer (see below), and homogenized using the Avestin EmulsiFlex-C5 homogenizer. Lysate was cleared by centrifugation at 20,000 *g* at 4°C for 20 min. For GST-tagged proteins, lysis buffer was GST-buffer (50 mM Tris–HCl, pH 7.5, 200 mM NaCl, 5 mM DTT) with 1 mM PMSF. GST-tagged proteins were precipitated from cleared lysate using Glutathione Sepharose™ 4 Fast Flow (GE Healthcare). The resin was washed with GST-buffer, and proteins were eluted with GST-buffer containing 20 mM reduced glutathione. Alternatively, proteins were released from the resin by digest with self-made GST-tagged 3C protease overnight. Lysis buffer for 6xHis-tagged proteins was either 1× PBS (137 mM NaCl, 2.7 mM KCl, 10.1 mM Na_2HPO_4, and 1.8 mM KH_2PO_4, pH 7.5) with 1 mM PMSF or 2× PBS with 2 mM 2-mercaptoethanol and 1 mM PMSF for hUbe1. Proteins with a 6xHis-tag were purified from cleared lysate using a HiTrap Talon affinity column (GE Healthcare). After binding, the resin was washed with 5–10 column volumes of PBS. Proteins were eluted with PBS containing 300 mM imidazole. The purification of untagged ubiquitin monomers was performed by acidic precipitation (Michel *et al*, 2018). 70% perchloric acid was added dropwise while stirring to the cleared lysate until a total final concentration of 0.7% was reached. The precipitate was cleared by centrifugation (20,000 *g* for 20 min at 4°C). The supernatant was recovered, and 10 M NaOH was titrated to adjust the pH to 7–8. All proteins were further purified by size-exclusion chromatography. The purity of all generated proteins was tested by SDS–PAGE and Coomassie staining.

Fluorescent labeling of ubiquitin

Ub(S20C) was fluorescently labeled using Alexa Fluor 488 C5 Maleimide (Invitrogen) or Alexa Fluor 647 C2 Maleimide (Invitrogen). Thiol groups were reduced with twofold molar excess of TCEP in 1× PBS for 10 min at RT. The sample was desalted using NAP5 columns and incubated with the fluorescent dye in fourfold molar excess in 1× PBS for 90 min in the dark. Subsequently, the sample was desalted twice using NAP5 columns equilibrated in 50 mM Tris–HCl, pH 8. The sample was concentrated in an Amicon Ultra concentrator (3K MWCO, Millipore). Final protein concentration was determined by Lowry assay. Where indicated, fluorescent ubiquitin was methylated using formaldehyde and cyanoborohydride as described elsewhere (Boersema *et al*, 2009). The reaction was quenched with ammonia and formic acid. Excess reagents were removed using Zeba Spin Desalting Columns (Thermo Scientific).

Assembly and purification of ubiquitin chains

Ubiquitin chains with proximal (i.e., C-terminal) hexahistidine-tag (6xHis) were assembled enzymatically *in vitro* typically in a total volume of 3–10 ml. Synthesis of K48-linked chains was performed with 1 μM E1 (hUbe1), 20 μM Cdc34, 900 μM ubiquitin, and 600 μM 6xHis-Ub in chain synthesis buffer (50 mM Tris–HCl, pH 8, 9 mM $MgCl_2$, 20 mM ATP, 0.9 mM DTT). K63-linked chains were assembled with 1 μM E1 (Ube1), 8 μM GST-Ubc13, 8 μM GST-Uev1a, 1.2 mM ubiquitin, and 0.8 mM 6xHis-Ub in chain synthesis buffer. Synthesis reactions for ubiquitin chain mixes used in the *in vitro* binding assay contained 200 μM Alexa 488-labeled 6xHis-Ub(S20C) and 1.8 mM ubiquitin instead (500 μl reaction volume). The synthesis reaction for a K48-/K63-branched ubiquitin trimer used for the generation of a spectral library contained 470 μM 6xHis-Ub(R54A), 515 μM Ub(K48R,K63R), 10 μM Ubc1(K93R), 8 μM GST-Ubc13, and 8 μM Gst-Uev1A in synthesis buffer (Fig EV3). All ubiquitin chain synthesis reactions were incubated at 37°C for 18 h. 6xHis-tagged chains were separated from the reaction mix by metal affinity chromatography using Talon resin. After elution, ubiquitin chain mixes for the *in vitro* binding assays were buffer-exchanged to ubiquitin-binding buffer (see below) using Zeba Spin Desalting Columns (Thermo Scientific). Ubiquitin chains from other reactions were separated by gel filtration (HiLoad 26/600 Superdex 75 pg, GE Healthcare) in 1× PBS with a low flow rate (0.3–0.5 ml/min). Fractions containing ubiquitin chains with a specific length were collected and concentrated using Amicon Ultra concentrators (Millipore).

In vitro ubiquitin-binding assay

GST-tagged proteins were immobilized on GSH resin and equilibrated in ubiquitin-binding buffer (50 mM Tris–HCl, pH 7.5, 150 mM NaCl, 1 g/l BSA). Binding of equal amounts of the respective proteins to the resin was validated by SDS–PAGE and Coomassie staining. 25 μl GSH resin with immobilized GST-proteins were incubated with 150 μl of the respective chain mix (25 μM monoubiquitin equivalent) for 2 h at 4°C on a rotating wheel. After the binding step, the samples were centrifuged at 800 *g* for 1 min, and the supernatant was collected. The resin was then washed two times with ubiquitin-binding buffer. Urea sample buffer (8 M urea,

200 mM Tris–HCl, pH 6.8, 5% SDS, 0.1 mM EDTA, 0.03% (w/v) bromophenol blue, 50 mM DTT) was added to the supernatant and to the washed resin, respectively. Samples were heated to 35°C for 5 min and analyzed by SDS–PAGE and fluorescence scan.

In vitro ubiquitination experiments

Single turnover ubiquitination reactions contained 10 μM acceptor ubiquitin as indicated, 1 μM Alexa 488-labeled monoubiquitin (Ub-S20C), and 0.2 μM hUbe1 in reaction buffer (50 mM Tris–HCl, pH 7.5, 4 mM $MgCl_2$, 4 mM ATP, and 0.5 mM DTT). Reactions were started by addition of the respective E2 enzyme (Ubc1 variants/Ube2K/ubc-20/GST-Ubc13/Ubc7) to a final concentration of 2 μM together with 2 μM cofactor where indicated (GST-Uev1a/soluble fragment of Cue1—residues 25-203). *In vitro* ubiquitination reactions in Fig 6B and C contained 6 μM Alexa 488-labeled monoubiquitin (Ub-S20C), 2 μM Alexa 647-labeled K63-Ub_3 (proximal Ub (S20C) with C-terminal 6xHis) and 2 μM full-length Ubc1 or Ubc1-ΔUBA in reaction buffer. *In vitro* ubiquitination reactions in Fig 6D contained 12 μM Alexa 488-labeled monoubiquitin (Ub-S20C), 3 μM K63-Ub_4 (C-terminal 6xHis) and 2 μM full-length Ubc1 or Ubc1-ΔUBA in reaction buffer.

At indicated time points, 15 μl samples were removed from the reaction mixes and added to 15 μl urea sample buffer (8 M urea, 200 mM Tris–HCl, pH 6.8, 5% SDS, 0.1 mM EDTA, 0.03% (w/v) bromophenol blue, 50 mM DTT). Samples were analyzed by SDS–PAGE and fluorescence scan using a Typhoon FLA 9500 laser scanner (GE Healthcare). All ubiquitination reactions with Ubc1 were performed with K93R mutants to block autoubiquitination and thus autoinhibition (Liess *et al*, 2019). For kinetic analyses, reactions were performed in triplicate. Line plots for all lanes in each scan were extracted using ImageJ. Data were then analyzed by using the Multipeak Fitting Package in Igor Pro. Peaks were approximated with Gaussian functions, and linear or constant baselines were automatically determined. Product intensity over total intensity per lane was plotted over time and approximated with a line function. Initial reaction rates were determined as slope of the function.

Expression of isotope-labeled ubiquitin for NMR

For the expression of ^{15}N-labeled ubiquitin monomers with and without 6xHis-tag, cells were grown in minimal medium containing 7.5 g/l Na_2HPO_4, 3 g/l KH_2PO_4, 0.5 g/l NaCl, 2 mM $MgSO_4$, 0.1 mM $CaCl_2$, 10 μM $FeSO_4$, 4 g/l glucose, 1 g/l $^{15}NH_4Cl$, vitamin mix, and trace element mix. Vitamin mix final concentrations were 1 mg/l D-biotin, 500 μg/l choline chloride, 500 μg/l folic acid, 1 mg/l myoinositol, 500 μg/l nicotinamide, 500 μg/l pantothenic acid, 500 μg/l pyridoxal hydrochloride, 50 μg/l riboflavin, and 500 μg/l thiamine hydrochloride. Trace element mix final concentrations were 50 mg/l EDTA, 8.3 mg/l $FeCl_3 \times 6H_2O$, 840 μg/l $ZnCl_2$, 0.13 mg/l $CuCl_2 \times 2H_2O$, 100 μg/l $CoCl_2 \times 6H_2O$, 100 μg/l H_3BO_3, and 16 μg/l $MnCl_2 \times 6\ H_2O$.

NMR spectroscopy

K48-Ub_2 (0.2 mM) and K63-Ub_2 (0.2 mM) carrying either a proximal or distal ^{15}N-labeled ubiquitin were prepared as described previously (von Delbrück *et al*, 2016). Diubiquitin was titrated with unlabeled UBA domain (aa151-215). UBA domain concentrations ranged from 0 to 1.6 mM. NMR experiments were performed at 298 K in NMR buffer (50 mM Na_2HPO_4 pH 7,100 mM NaCl, and 5% D2O) and monitored by [^{15}N, ^{1}H]-heteronuclear single quantum coherence spectroscopy (HSQC) spectra. To determine the K_D value for proximal and distal ubiquitin moieties, a fitting model for two independent binding sites with different affinities was used (Raasi *et al*, 2005). NMR spectra were acquired on Bruker Avance spectrometers operating at proton Larmor frequencies ranging from 600 to 950 MHz, equipped with 5-mm $^{1}H\{^{13}C/^{15}N\}$ cryogenic probes. Samples were measured in salt-tolerant NMR tubes in a total volume of 350–400 μl. Chemical shift referencing was performed with 4,4-dimethyl-4-silapentane-1-sulfonate (DSS). Spectra were processed using the TopSpin software provided by Bruker and analyzed using SPARKY 3.13 software or NMRFAM-SPARKY (Lee *et al*, 2015).

Mass spectrometric analyses

Spectral library generation

A spectral library for K48/K63-branched chains was obtained from an enzymatically assembled branched ubiquitin trimer (Fig EV3). The purified ubiquitin trimer was incubated with trypsin in a mass ratio of 50:1 for an overnight incubation at RT. Peptides were separated by reverse-phase chromatography and analyzed on a Q Exactive Plus (Thermo Fisher) with the following settings: MS1: 60,000 resolution; AGC target 3e6; Max IT 10 ms; MS2: 16,000 resolution; MaxIT 60ms; AGC 4e5. The data were extracted using MQ and searched against the yeast UniProt database from 2014 plus version of the additional expected sequences as a result of the genomic modifications. The data were analyzed with MaxQuant 1.6.3.4 (Cox & Mann, 2008). MaxQuant settings were as follows: multiplicity 1; fixed modification: carbamidomethyl (C); protease: trypsin with allowed cleavages after proline; variable modifications: acetylation (nterm), oxidation (M), and GlyGly (K); PSM FDR: 0.01; and protein FDR: 0.01. Ubiquitin-related peptides with the highest score were selected and used as a spectral library for all subsequent PRM analyses.

Yeast sample preparation for mass spectrometry measurements

To investigate the abundance of K48/K63-branched chains in *S. cerevisiae*, yeast strains were transformed with expression plasmids for 10xHis-Ub(R54A) and grown in either unlabeled or Lys8-labeled minimal media. For the proteomic shotgun experiments, arginine auxotroph yeast cells (Δ*arg4::kanMX6*) were grown in either unlabeled or Lys8- and Arg10-labeled minimal media. Equal amounts of cells (400 ml at 0.6 OD_{600}/ml) from different conditions and with different labels were combined, mixed, and centrifuged. Pellets of the combined cells were flash-frozen in liquid nitrogen and stored at −80°C overnight. Pellets used for branched chain detection were resuspended in denaturing lysis buffer (6 M GdmCl, 100 mM HEPES, pH 7.5, 300 mM NaCl, 10 mM chloroacetamide, 1 mM PMSF) for mechanical lysis with glass beads. Additional lysis buffer containing Triton X-100 was added to a final concentration of 0.2% Triton X-100 for solubilization at 4°C for 30 min. The lysate was cleared by centrifugation and incubated with Ni-NTA resin. After 2.5 h, the resin was washed twice with wash buffer 1 (8 M urea, 100 mM HEPES, pH7.5, 300 mM NaCl, 0.2%

Triton X-100, and 10 mM chloroacetamide) and twice with wash buffer 2 (8 M urea, 100 mM HEPES, pH7.5, 300 mM NaCl, 0.2% Triton X-100, 0.2% SDS, and 10mM chloroacetamide). Finally, protein was eluted using elution buffer (8 M urea, 100 mM HEPES, pH7.5, 300 mM NaCl, 350 mM imidazole, 0.2% Triton X-100, 0.2% SDS, and 10 mM chloroacetam ide) and subjected to methanol/chloroform extraction as described elsewhere (Wessel & Flügge, 1984). The protein pellet was resuspended in denaturation buffer (6 M urea, 2 M thiourea, and 10 mM HEPES, pH 8.0). 0.5 μg LysC protease was added and incubated for 3 h at RT while shaking. The sample was diluted with 50 mM ammonium bicarbonate buffer before adding 0.5 μg trypsin for digest at RT overnight. For the proteomic shotgun experiments, pellets were resuspended in 500 μl lysis buffer (50mM ABC, 10mM DTT, protease inhibitor cocktail EDTA-free, and 1 mM PMSF) for mechanical lysis with glass beads. After lysis, 1 ml solubilization buffer was added (25 mM ABC, 10 mM DTT, and 4.5% SDS) and samples were boiled at 95°C for 5 min. Lysates were cleared by centrifugation, alkylated with iodoacetamide, and quenched with DTT. The samples were then further processed using solid-phase-enhanced sample preparation (Hughes *et al*, 2019). In short, hydrophilic paramagnetic beads were used to recover protein from the lysate and a peptide digest was performed on-bead using LysC and trypsin. Subsequently, peptides were dried and resuspended in a high pH buffer A (5 mM ammonium formate, 2% ACN) and subjected to offline high pH reverse-phase fractionation (Bekker-Jensen *et al*, 2017) by HPLC (Thermo Fisher Dionex Ultimate 3000) on a XBridge Peptide BEH C18 (130 Å, 3.5 μm; 2.1 mm × 250 mm) column (Waters) with a multistep gradient from 0 to 60% high pH buffer B (5 mM ammonium formate, 90% ACN) over 96 min. In total, 96 fractions were collected (1 fraction/min) und automatically pooled into 24 fractions. Subsequently, 24 fractions ("Ubc1-EA" samples) or 12 pooled fractions ("heatshock" and "Δubc4" samples) were subjected for measurement by mass spectrometry.

Mass spectrometry measurements and settings

For the targeted proteomic measurements, peptides were separated by reverse-phase chromatography on an effective 80 min gradient (0, 10, 60, 70, and 80 min with 0, 4, 20, 30, and 50% of 90% acetonitrile) and analyzed on a Q Exactive HFx (Thermo Fisher) in positive polarity mode. The PRM settings were as follows: 30k resolution; 2e5 AGC target; 1.6 *m/z* isolation window; and 100 ms max ion injection time. In addition, a Top-2 method was integrated into the same run with the following settings: MS1: 15k resolution; AGC target: 3e6; Max IT: 10 ms; MS2: 7 500 resolution; AGC target: 1e5; MaxIT: 12 ms; isolation window: 1.3 *m/z*; minimum AGC target: 1e4; dynamic exclusion: 30 s; and nCE = 26.

Shotgun proteomic measurements were separated by reverse-phase chromatography on an effective 21 min ("Ubc1-EA") or 35 min ("heatshock" and "Δubc4") gradient. "Ubc1-EA" samples were analyzed on a Thermo Fisher Q Exactive HFx instrument in positive polarity mode with the following additional settings: MS1: 60k resolution; AGC target: 2e5; MaxIT: 50 ms; MS2: Top20; 15k resolution; AGC target: 2e5; nCE = 26; MaxIT: 40ms; isolation window: 1.3 *m/z*; minimum AGC target: 1e4; dynamic exclusion: 30 s. Heatshock and Δubc4 samples were analyzed on Thermo-Fisher Exploris 480 instrument with the following settings: Faims with three cycle CVs (−40,-55, and −70); MS1: 60k resolution; Norm AGC target: 300%; AGC target = custom; MS2: 15k resolution; normalized AGC target = 200%; MaxIT = custom; and nCE = 28.

Data analysis of targeted mass spectrometric measurements

Traces of all fragments from precursors in the spectral library were extracted from all raw files using the Thermo MSFileReader and the MSFileReader.py bindings written by François Allen. For each scan, the normalized spectral contrast angle (SCN) was calculated (Toprak *et al*, 2014). Peaks were manually selected with an unpublished in-house PRM-data visualization tool called Vali. Ratios were extracted from the slope of a linear model on extracted intensity pairs of the heavy and light channel for each peak across all fragments.

The data were analyzed in parallel with MaxQuant (v.1.6.17.0) against the UniProt yeast protein sequence database from 2014. MaxQuant settings were as follows: multiplicity 2 with Lys8 as a heavy label; fixed modification: carbamidomethyl (C); protease: trypsin with allowed cleavages after proline; variable modifications: acetylation (nterm) and oxidation (M); PSM FDR: 0.01; protein FDR: 0.01. Unnormalized peptide ratios as reported by MaxQuant were read in and log2-transformed distributions were centered to the median. The corresponding shifts were subsequently applied on calculated ratios from the PRM measurements. The shotgun and PRM log2-transformed ratios were visualized together using the ggplot2 packages in R (3.6.3).

Data analysis of shotgun mass spectrometric measurements

Rawfiles acquired with Faims were converted to CV-specific mzxml files (Hebert *et al*, 2018). All Rawfiles or mzxml files were analyzed in MaxQuant v.1.6.17.0 with the following additional settings: multiplicity 2, Lys8 and Arg10 as heavy label; trypsin/P; carbamidomethylation (C) as fixed modification; oxidation (M), acetyl (protein n-terminal), and deamidation (NQ) as variable modifications; match between runs enabled; and re-Quantify enabled. *P*-values were calculated from reverse and forward experiments using the Significance B approach (Cox & Mann, 2008). Genes were considered as significantly different in their protein log2-fold-changes if they had a *P*-value < 0.01 and showed the same fold-change trend in both experiments. These data were then further analyzed using YeastMine (Balakrishnan *et al*, 2012).

Data availability

The mass spectrometry proteomics data have been deposited to the ProteomeXchange Consortium via the PRIDE (Perez-Riverol *et al*, 2019) partner repository [http://www.proteomexchange.org/] with the dataset identifiers PXD018651 and PXD022621. A PDB file containing the model of Ube2K in complex with ubiquitin is available from the authors upon request.

Expanded View for this article is available online.

Acknowledgements

This work was funded by the Deutsche Forschungsgemeinschaft (SO 271/9-1, DO 545/17-1). B.A.S. was supported by the Max Planck Gesellschaft. We thank

Dr. Janine Kirstein for providing a cDNA library for the cloning of ubc-20. We would also like to express our gratitude to Dr. David Krist, Dr. Jérôme Basquin, and Dr. Rajan Prabu for assistance with preliminary structural experiments, which informed the model building. Furthermore, we thank Tommaso Mari for the assistance with sample preparation for mass spectrometry. We are also grateful to Dr. Oliver Daumke for valuable comments on the paper.

Author contributions

LP, EJ, HZ, and AK designed the study, conducted experiments, and interpreted data. AW, KB, and MvD. created unique reagents for the study. TS, VD, MS, BAS, and FL designed experiments and interpreted data. LP, TS, EJ, and AW wrote the manuscript.

Conflict of interest

The authors declare that they have no conflict of interest.

References

Balakrishnan R, Park J, Karra K, Hitz BC, Binkley G, Hong EL, Sullivan J, Micklem G, Michael Cherry J (2012) YeastMine—an integrated data warehouse for *Saccharomyces cerevisiae* data as a multipurpose tool-kit. *Database* 2012: bar062

Bedalov A, Hirao M, Posakony J, Nelson M, Simon JA (2003) NAD+-dependent deacetylase Hst1p controls biosynthesis and cellular NAD+ levels in *Saccharomyces cerevisiae*. *Mol Cell Biol* 23: 7044 – 7054

Bekker-Jensen DB, Kelstrup CD, Batth TS, Larsen SC, Haldrup C, Bramsen JB, Sørensen KD, Høyer S, Ørntoft TF, Andersen CL *et al* (2017) An optimized shotgun strategy for the rapid generation of comprehensive human proteomes. *Cell Systems* 4: 587 – 599.e4

Boersema PJ, Raijmakers R, Lemeer S, Mohammed S, Heck AJR (2009) Multiplex peptide stable isotope dimethyl labeling for quantitative proteomics. *Nat Protoc* 4: 484 – 494

Branigan E, Plechanovová A, Jaffray EG, Naismith JH, Hay RT (2015) Structural basis for the RING-catalyzed synthesis of K63-linked ubiquitin chains. *Nat Struct Mol Biol* 22: 597 – 602

Clague MJ, Heride C, Urbé S (2015) The demographics of the ubiquitin system. *Trends Cell Biol* 25: 417 – 426

Cook BW, Barber KR, Shilton BH, Shaw GS (2015) The HIP2~ubiquitin conjugate forms a non-compact monomeric thioester during Di-ubiquitin synthesis. *PLoS One* 10: e0120318

Cook BW, Lacoursiere RE, Shaw GS (2020) Recruitment of ubiquitin within an E2 chain elongation complex. *Biophys J* 118: 1679 – 1689

Cox J, Mann M (2008) MaxQuant enables high peptide identification rates, individualized p.p.b.-range mass accuracies and proteome-wide protein quantification. *Nat Biotechnol* 26: 1367 – 1372

von Delbrück M, Kniss A, Rogov VV, Pluska L, Bagola K, Löhr F, Güntert P, Sommer T, Dötsch V (2016) The CUE domain of Cue1 aligns growing ubiquitin chains with Ubc7 for rapid elongation. *Mol Cell* 62: 918 – 928

Emmerich CH, Ordureau A, Strickson S, Arthur JSC, Pedrioli PGA, Komander D, Cohen P (2013) Activation of the canonical IKK complex by K63/M1-linked hybrid ubiquitin chains. *Proc Natl Acad Sci USA* 110: 15247 – 15252

Fatima A, Irmak D, Noormohammadi A, Rinschen MM, Das A, Leidecker O, Schindler C, Sánchez-Gaya V, Wagle P, Pokrzywa W *et al* (2020) The ubiquitin-conjugating enzyme UBE2K determines neurogenic potential through histone H3 in human embryonic stem cells. *Commun Biol* 3: 262

Friedlander R, Jarosch E, Urban J, Volkwein C, Sommer T (2000) A regulatory link between ER-associated protein degradation and the unfolded-protein response. *Nat Cell Biol* 2: 379 – 384

Gack MU, Shin YC, Joo C-H, Urano T, Liang C, Sun L, Takeuchi O, Akira S, Chen Z, Inoue S *et al* (2007) TRIM25 RING-finger E3 ubiquitin ligase is essential for RIG-I-mediated antiviral activity. *Nature* 446: 916 – 920

Girard JR, Tenthorey JL, Morgan DO (2015) An E2 accessory domain increases affinity for the anaphase-promoting complex and ensures E2 competition. *J Biol Chem* 290: 24614 – 24625

Gueldener U (2002) A second set of loxP marker cassettes for Cre-mediated multiple gene knockouts in budding yeast. *Nucleic Acids Res* 30: e23

Gulia R, Sharma R, Bhattacharyya S (2017) A critical role for ubiquitination in the endocytosis of glutamate receptors. *J Biol Chem* 292: 1426 – 1437

Hebert AS, Prasad S, Belford MW, Bailey DJ, McAlister GC, Abbatiello SE, Huguet R, Wouters ER, Dunyach J-J, Brademan DR *et al* (2018) Comprehensive single-shot proteomics with FAIMS on a hybrid orbitrap mass spectrometer. *Anal Chem* 90: 9529 – 9537

Hershko A, Ciechanover A (1998) The ubiquitin system. *Annu Rev Biochem* 67: 425 – 479

Hiraishi H, Mochizuki M, Takagi H (2006) Enhancement of stress tolerance in *Saccharomyces cerevisiae* by overexpression of ubiquitin ligase Rsp5 and ubiquitin-conjugating enzymes. *Biosci Biotechnol Biochem* 70: 2762 – 2765

Hong NH, Tak YJ, Rhim H, Kang S (2019) Hip2 ubiquitin-conjugating enzyme has a role in UV-induced G1/S arrest and re-entry. *Genes Genom* 41: 159 – 166

Hughes CS, Moggridge S, Müller T, Sorensen PH, Morin GB, Krijgsveld J (2019) Single-pot, solid-phase-enhanced sample preparation for proteomics experiments. *Nat Protoc* 14: 68 – 85

Ibarra R, Sandoval D, Fredrickson EK, Gardner RG, Kleiger G (2016) The San1 ubiquitin ligase functions preferentially with ubiquitin-conjugating enzyme Ubc1 during protein quality control. *J Biol Chem* 291: 18778 – 18790

Jiao R, Lubanova L, Waldner A, Fu A, Xiao L, Harkness T, Arnason T (2016) The ubiquitin-conjugating enzyme, Ubc1, indirectly regulates SNF1 kinase activity via Forkhead-dependent transcription. *Microb Cell* 3: 540 – 553

Kalchman MA, Graham RK, Xia G, Koide HB, Hodgson JG, Graham KC, Goldberg YP, Gietz RD, Pickart CM, Hayden MR (1996) Huntingtin is ubiquitinated and interacts with a specific ubiquitin-conjugating enzyme. *J Biol Chem* 271: 19385 – 19394

Kelley LA, Mezulis S, Yates CM, Wass MN, Sternberg MJE (2015) The Phyre2 web portal for protein modeling, prediction and analysis. *Nat Protoc* 10: 845 – 858

Kniss A, Schuetz D, Kazemi S, Pluska L, Spindler PE, Rogov VV, Husnjak K, Dikic I, Güntert P, Sommer T *et al* (2018) Chain assembly and disassembly processes differently affect the conformational space of ubiquitin chains. *Structure* 26: 249 – 258.e4

Ko S, Kang GB, Song SM, Lee J-G, Shin DY, Yun J-H, Sheng Y, Cheong C, Jeon YH, Jung Y-K *et al* (2010) Structural basis of E2–25K/UBB +1 interaction leading to proteasome inhibition and neurotoxicity. *J Biol Chem* 285: 36070 – 36080

Kozlov G, Nguyen L, Lin T, De Crescenzo G, Park M, Gehring K (2007) Structural basis of ubiquitin recognition by the ubiquitin-associated (UBA) domain of the ubiquitin ligase EDD. *J Biol Chem* 282: 35787 – 35795

Lange OF, Lakomek N-A, Fares C, Schroder GF, Walter KFA, Becker S, Meiler J, Grubmuller H, Griesinger C, de Groot BL (2008) Recognition dynamics up to microseconds revealed from an RDC-derived ubiquitin ensemble in solution. *Science* 320: 1471 – 1475

Lauwers E, Jacob C, André B (2009) K63-linked ubiquitin chains as a specific signal for protein sorting into the multivesicular body pathway. *J Cell Biol* 185: 493 – 502

Lee W, Tonelli M, Markley JL (2015) NMRFAM-SPARKY: enhanced software for biomolecular NMR spectroscopy. *Bioinformatics* 31: 1325 – 1327

Lee J-G, Youn H-S, Kang JY, Park S-Y, Kidera A, Yoo YJ, Eom SH (2018) Crystal structure of the Ube2K/E2-25K and K48-linked di-ubiquitin complex provides structural insight into the mechanism of K48-specific ubiquitin chain synthesis. *Biochem Biophys Res Comm* 506: 102 – 107

Liess AKL, Kucerova A, Schweimer K, Yu L, Roumeliotis TI, Diebold M, Dybkov O, Sotriffer C, Urlaub H, Choudhary JS *et al* (2019) Autoinhibition mechanism of the ubiquitin-conjugating enzyme UBE2S by autoubiquitination. *Structure* 27: 1195 – 1210.e7

Liu P, Gan W, Su S, Hauenstein AV, Fu T, Brasher B, Schwerdtfeger C, Liang AC, Xu M, Wei W (2018) K63-linked polyubiquitin chains bind to DNA to facilitate DNA damage repair. *Sci Signal* 11: eaar8133

Longtine MS, McKenzie A, Demarini DJ, Shah NG, Wach A, Brachat A, Philippsen P, Pringle JR (1998) Additional modules for versatile and economical PCR-based gene deletion and modification in *Saccharomyces cerevisiae*. *Yeast* 14: 953 – 961

Madeira F, Park Ym, Lee J, Buso N, Gur T, Madhusoodanan N, Basutkar P, Tivey ARN, Potter SC, Finn RD *et al* (2019) The EMBL-EBI search and sequence analysis tools APIs in 2019. *Nucleic Acids Res* 47: W636 – W641

Medintz I, Jiang H, Michels CA (1998) The role of ubiquitin conjugation in glucose-induced proteolysis of *Saccharomyces* maltose permease. *J Biol Chem* 273: 34454 – 34462

Meena RC, Thakur S, Nath S, Chakrabarti A (2011) Tolerance to thermal and reductive stress in *Saccharomyces cerevisiae* is amenable to regulation by phosphorylation-dephosphorylation of ubiquitin conjugating enzyme 1 (Ubc1) S97 and S115: regulation of stress tolerance in *S. cerevisiae*. *Yeast* 28: 783 – 793

Melo R, Fieldhouse R, Melo A, Correia J, Cordeiro M, Gümüş Z, Costa J, Bonvin A, Moreira I (2016) A machine learning approach for hot-spot detection at protein-protein interfaces. *Int J Mol Sci* 17: 1215

Merkley N, Shaw GS (2004) Solution structure of the flexible class II ubiquitin-conjugating enzyme Ubc1 provides insights for polyubiquitin chain assembly. *J Biol Chem* 279: 47139 – 47147

Merkley N, Barber KR, Shaw GS (2005) Ubiquitin manipulation by an E2 conjugating enzyme using a novel covalent intermediate. *J Biol Chem* 280: 31732 – 31738

Meyer H-J, Rape M (2014) Enhanced protein degradation by branched ubiquitin chains. *Cell* 157: 910 – 921

Michel MA, Komander D, Elliott PR (2018) Enzymatic assembly of ubiquitin chains. In *The Ubiquitin Proteasome System*, Mayor T, Kleiger G (eds), pp 73 – 84. New York, NY: Springer New York.

Michielssens S, Peters JH, Ban D, Pratihar S, Seeliger D, Sharma M, Giller K, Sabo TM, Becker S, Lee D *et al* (2014) A designed conformational shift to control protein binding specificity. *Angew Chem Int Ed* 53: 10367 – 10371

Middleton AJ, Day CL (2015) The molecular basis of lysine 48 ubiquitin chain synthesis by Ube2K. *Sci Rep* 5: 16793

Moreira IS, Koukos PI, Melo R, Almeida JG, Preto AJ, Schaarschmidt J, Trellet M, Gümüş ZH, Costa J, Bonvin AMJJ (2017) SpotOn: high accuracy identification of protein-protein interface hot-spots. *Sci Rep* 7: 8007

Mühlhofer M, Berchtold E, Stratil CG, Csaba G, Kunold E, Bach NC, Sieber SA, Haslbeck M, Zimmer R, Buchner J (2019) The heat shock response in yeast maintains protein homeostasis by chaperoning and replenishing proteins. *Cell Rep* 29: 4593 – 4607.e8

Ohtake F, Saeki Y, Ishido S, Kanno J, Tanaka K (2016) The K48–K63 branched ubiquitin chain regulates NF-κB signaling. *Mol Cell* 64: 251 – 266

Ohtake F, Tsuchiya H, Saeki Y, Tanaka K (2018) K63 ubiquitylation triggers proteasomal degradation by seeding branched ubiquitin chains. *Proc Natl Acad Sci USA* 115: E1401 – E1408

Ong S-E, Blagoev B, Kratchmarova I, Kristensen DB, Steen H, Pandey A, Mann M (2002) Stable isotope labeling by amino acids in cell culture, SILAC, as a simple and accurate approach to expression proteomics. *Mol Cell Proteomics* 1: 376 – 386

Pastushok L, Moraes TF, Ellison MJ, Xiao W (2005) A single Mms2 "Key" residue insertion into a Ubc13 Pocket determines the interface specificity of a human Lys ^{63} ubiquitin conjugation complex. *J Biol Chem* 280: 17891 – 17900

Perez-Riverol Y, Csordas A, Bai J, Bernal-Llinares M, Hewapathirana S, Kundu DJ, Inuganti A, Griss J, Mayer G, Eisenacher M *et al* (2019) The PRIDE database and related tools and resources in 2019: improving support for quantification data. *Nucleic Acids Res* 47: D442 – D450

de Pril R, Fischer DF, Roos RAC, van Leeuwen FW (2007) Ubiquitin-conjugating enzyme E2–25K increases aggregate formation and cell death in polyglutamine diseases. *Mol Cell Neurosci* 34: 10 – 19

Raasi S, Varadan R, Fushman D, Pickart CM (2005) Diverse polyubiquitin interaction properties of ubiquitin-associated domains. *Nat Struct Mol Biol* 12: 708 – 714

Rodrigo-Brenni MC, Morgan DO (2007) Sequential E2s drive polyubiquitin chain assembly on APC targets. *Cell* 130: 127 – 139

Rodrigo-Brenni MC, Foster SA, Morgan DO (2010) Catalysis of lysine 48-specific ubiquitin chain assembly by residues in E2 and ubiquitin. *Mol Cell* 39: 548 – 559

Rout MK, Lee BL, Lin A, Xiao W, Spyracopoulos L (2018) Active site gate dynamics modulate the catalytic activity of the ubiquitination enzyme E2–25K. *Sci Rep* 8: 7002

Seufert W, McGrath JP, Jentsch S (1990) UBC1 encodes a novel member of an essential subfamily of yeast ubiquitin-conjugating enzymes involved in protein degradation. *EMBO J* 9: 4535 – 4541

Shapovalov MV, Dunbrack RL (2011) A smoothed backbone-dependent rotamer library for proteins derived from adaptive kernel density estimates and regressions. *Structure* 19: 844 – 858

Shieh H-L, Chen Y, Brown CR, Chiang H-L (2001) Biochemical analysis of fructose-1,6-bisphosphatase import into vacuole import and degradation vesicles reveals a role for *UBC1* in vesicle biogenesis. *J Biol Chem* 276: 10398 – 10406

Song S, Kim S-Y, Hong Y-M, Jo D-G, Lee J-Y, Shim SM, Chung C-W, Seo SJ, Yoo YJ, Koh J-Y *et al* (2003) Essential role of E2–25K/Hip-2 in mediating amyloid-β neurotoxicity. *Mol Cell* 12: 553 – 563

Spence J, Sadis S, Haas AL, Finley D (1995) A ubiquitin mutant with specific defects in DNA repair and multiubiquitination. *Mol Cell Biol* 15: 1265 – 1273

Stewart MD, Ritterhoff T, Klevit RE, Brzovic PS (2016) E2 enzymes: more than just middle men. *Cell Res* 26: 423 – 440

Stoll KE, Brzovic PS, Davis TN, Klevit RE (2011) The essential Ubc4/Ubc5 function in yeast is HECT E3-dependent, and RING E3-dependent pathways require only monoubiquitin transfer by Ubc4. *J Biol Chem* 286: 15165 – 15170

Swatek KN, Komander D (2016) Ubiquitin modifications. *Cell Res* 26: 399 – 422

Tkach JM, Yimit A, Lee AY, Riffle M, Costanzo M, Jaschob D, Hendry JA, Ou J, Moffat J, Boone C *et al* (2012) Dissecting DNA damage response pathways by analysing protein localization and abundance changes during DNA replication stress. *Nat Cell Biol* 14: 966 – 976

Toprak UH, Gillet LC, Maiolica A, Navarro P, Leitner A, Aebersold R (2014) Conserved peptide fragmentation as a benchmarking tool for mass spectrometers and a discriminating feature for targeted proteomics. *Mol Cell Proteomics* 13: 2056 – 2071

Valimberti I, Tiberti M, Lambrughi M, Sarcevic B, Papaleo E (2015) E2 superfamily of ubiquitin-conjugating enzymes: constitutively active or activated through phosphorylation in the catalytic cleft. *Sci Rep* 5: 14849

Wang C, Deng L, Hong M, Akkaraju GR, Inoue J, Chen ZJ (2001) TAK1 is a ubiquitin-dependent kinase of MKK and IKK. *Nature* 412: 346 – 351

Wang Y, Tang C, Wang E, Wang J (2014) PolyUbiquitin chain linkage topology selects the functions from the underlying binding landscape. *PLoS Comput Biol* 10: e1003691

Watson ER, Grace CRR, Zhang W, Miller DJ, Davidson IF, Prabu JR, Yu S, Bolhuis DL, Kulko ET, Vollrath R *et al* (2019) Protein engineering of a ubiquitin-variant inhibitor of APC/C identifies a cryptic K48 ubiquitin chain binding site. *Proc Natl Acad Sci USA* 116: 17280 – 17289

Weber A, Cohen I, Popp O, Dittmar G, Reiss Y, Sommer T, Ravid T, Jarosch E (2016) Sequential poly-ubiquitylation by specialized conjugating enzymes expands the versatility of a quality control ubiquitin ligase. *Mol Cell* 63: 827 – 839

Welker S, Rudolph B, Frenzel E, Hagn F, Liebisch G, Schmitz G, Scheuring J, Kerth A, Blume A, Weinkauf S *et al* (2010) Hsp12 is an intrinsically unstructured stress protein that folds upon membrane association and modulates membrane function. *Mol Cell* 39: 507 – 520

Wertz IE, Newton K, Seshasayee D, Kusam S, Lam C, Zhang J, Popovych N, Helgason E, Schoeffler A, Jeet S *et al* (2015) Phosphorylation and linear ubiquitin direct A20 inhibition of inflammation. *Nature* 528: 370 – 375

Wessel D, Flügge UI (1984) A method for the quantitative recovery of protein in dilute solution in the presence of detergents and lipids. *Anal Biochem* 138: 141 – 143

Wilson RC, Hughes RC, Flatt JW, Meehan EJ, Ng JD, Twigg PD (2009) Structure of full-length ubiquitin-conjugating enzyme E2–25K (Huntingtin-interacting protein 2). *Acta Crystallogr Sect F Struct Biol Cryst Commun* 65: 440 – 444

Wright JD, Mace PD, Day CL (2016) Noncovalent ubiquitin interactions regulate the catalytic activity of ubiquitin writers. *Trends Biochem Sci* 41: 924 – 937